BULK AND INTERFACE IMPERFECTIONS
IN SEMICONDUCTORS

Illinois University at
Urbana-Champaign

November 1976

RADC-TR-76-341
Interim Technical Report No. 3
November 1976

BULK AND INTERFACE IMPERFECTIONS IN
SEMICONDUCTORS

University of Illinois

Approved for public release; distribution unlimited.

ROME AIR DEVELOPMENT CENTER
SIR FORCE SYSTEMS COMMAND
GRIFFISS AIR FORCE BASE, NEW YORK 13441
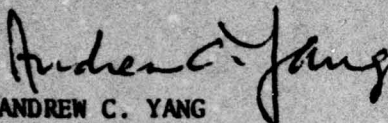
ADA035151

DDC
FEB 1977
RECEIVED
B

Dr. C. T. Sah is the responsible investigator for this contract. Andrew C. Yang (ETSD), is the RADC Project Engineer.

This report has been reviewed by the RADC Information Office (OI) and is releasable to the National Technical Information Service (NTIS). At NTIS it will be releasable to the general public, including foreign nations.

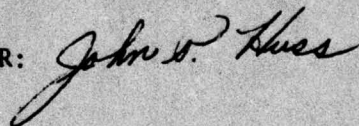This technical report has been reviewed and approved for publication.

APPROVED: *Andrew C. Yang*

ANDREW C. YANG
Project Engineer

APPROVED: *Robert M. Barrett*

ROBERT M. BARRETT
Director
Solid State Sciences Division

FOR THE COMMANDER: *John P. Huss*

Plans Office

R   DI   76-559

REPORT DOCUMENTATION PAGE	READ INSTRUCTIONS BEFORE COMPLETING FORM

1. REPORT NUMBER	2. GOVT ACCESSION NO.	3. RECIPIENT'S CATALOG NUMBER
RADC-TR-76-341		

4. TITLE *(and Subtitle)*	5. TYPE OF REPORT & PERIOD COVERED
BULK AND INTERFACE IMPERFECTIONS IN SEMICONDUCTORS	Scientific Report No. 3 Interim (Sep 74-Sep 75)
	6. PERFORMING ORG. REPORT NUMBER

7. AUTHOR(s)	8. CONTRACT OR GRANT NUMBER(s)
C. T. Sah	F19628-72-C-0199

9. PERFORMING ORGANIZATION NAME AND ADDRESS	10. PROGRAM ELEMENT, PROJECT, TASK AREA & WORK UNIT NUMBERS
University of Illinois Dept of Electrical Engineering 155 Electrical Engineering Bldg Urbana, Illinois 61801	61102F 56210702

11. CONTROLLING OFFICE NAME AND ADDRESS	12. REPORT DATE
Deputy for Electronic Technology(RADC/ETSD) Hanscom AFB, Massachusetts 01731 Monitor/Andrew C. Yang	November 1976
	13. NUMBER OF PAGES
	71

14. MONITORING AGENCY NAME & ADDRESS*(if different from Controlling Office)*	15. SECURITY CLASS. *(of this report)*
	Unclassified
	15a. DECLASSIFICATION/DOWNGRADING SCHEDULE

16. DISTRIBUTION STATEMENT *(of this Report)*

Approved for public release; distribution unlimited.

17. DISTRIBUTION STATEMENT *(of the abstract entered in Block 20, if different from Report)*

18. SUPPLEMENTARY NOTES

19. KEY WORDS *(Continue on reverse side if necessary and identify by block number)*

Defects	Silicon vacancy	Diodes
Diffusion	Interface states	pn junctions
Recombination center	Impurities	Schottky barriers
Silicon	Semiconductor	MOS capacitance

20. ABSTRACT *(Continue on reverse side if necessary and identify by block number)*

Charges trapped at imperfection centers can be detected by observing the slow time dependences of the high-frequency small-signal capacitance or the generation-recombination-trapping current of a semiconductor space charge region. Detection sensitivity of 10^{10} electronic charges per cm^3 in a volume of $(10^{-4}cm) \times (10^{-3}cm^2)$ of 10^3 electronic charges can be achieved with simple commercial equipments. This technique has been used to study the temperature, electric field and photon energy dependences of the thermal, optical and Auger-

DD $\frac{FORM}{1\ JAN\ 73}$ 1473   EDITION OF 1 NOV 65 IS OBSOLETE

impact emission and capture of electrons and holes at impurity and defect centers in bulk and surface space charge regions of semiconductors. It is also used to study the generation, annealing and diffusion kinetics of these centers and to monitor the silicon integrated circuit fabrication processes. The principle of this technique is described and experimental examples are given to illustrate the applications of the technique.

TABLE OF CONTENTS

LIST OF FIGURES

LIST OF FIGURES (Cont'd)

BULK AND INTERFACE IMPERFECTIONS IN SEMICONDUCTORS[+]

C. T. Sah

I. INTRODUCTION

Imperfections in solids may be dynamic or static. They perturb the periodicity of the crystal. This paper will review some new measurement techniques that determine the properties of static imperfections such as chemical impurities and physical defects from self interstitials and vacancies. It is well known that imperfections are important because they control the electrical, optical, thermal and mechanical properties of solids.

The impurity and defect imperfection centers affect both the electrical and optical characteristics of solid state devices such as the bipolar transistor, the MOS field-effect transistor, the light emitting diode, the junction laser, and the tunnel diode. For example, the quantum efficiency of the light emitting diode and the junction laser is reduced by the presence of nonradiative impurity and defect recombination centers. For another example, the charge transfer efficiency in the charge coupled devices is affected by the generation of electron-hole pairs at the imperfection centers located in the surface space charge region. The efficiency is also reduced by the recombination or trapping of electrons and holes at the fast interface states located at the oxide-silicon interface.

The presence of the imperfections as recombination centers will improve certain device characteristics in some cases. For example, gold impurity has been used as recombination centers to reduce the minority carrier lifetime and to increase the switching speed of silicon diodes and transistors. The technique of controlling lifetime and switching time was first introduced by members of the Bell Telephone Laboratories in 1960 for silicon diodes and by members of the

---

Fairchild Semiconductor Laboratories in 1961 for diffused silicon transistors. Radiative recombination centers can also be useful in giving different colors in light emitting diodes and in phosphors.

The history of research in semiconductor physics and solid state electronics is filled with novel experimental techniques to control the concentration of the impurity and defect centers, to measure their electrical and optical properties and to physically understand and to theoretically predict these electrical, optical as well as thermal properties from first principles.

Impurities and defects are usually present in minute quantitites in most practical situations. The very low concentration presents a major challenge to detect their presence and to measure their properties accurately.

Almost all of the earlier data were obtained on uniform samples from the temperature dependences of the Hall effect and electrical conductivity and from the infrared absorption spectra. The Hall and conductivity measurements are tedious and require liquid helium temperature apparatus. The data give the thermal activation energies of trapped electrons or holes at the imperfection centers. The Hall data also give the concentration of the imperfection centers and the conductivity data also give the Hall mobilities.

The concentration in the sample must be high to give measureable effects in the Hall effect experiments. Even at high concentrations, the results are usually not too accurate. Part of this inaccuracy comes from the uncertainty in the theoretical model of the bound electron or hole states in semiconductors, such as the unknown excited states and energy level degeneracy factors.

Results of the thermal activation energy measurements in silicon are shown in Figure 1 which is taken from Simon Sze's book published in 1969 (Wiley). More recent results are tabulated and given in figures similar to Figure 1 by A. G. Milnes in his 1973 book which surveys the properties of imperfections in

-2-

semiconductors (Wiley 1973). For the deep energy levels, most of the data listed in Figure 1 are in some doubt, except perhaps the data for gold and one or two other impurities. This is because of substantial differences in the results obtained by various methods at different laboratories. A similar lack of agreement of energy levels also appears in Ge and III-V compounds. One of the most serious difficulties which contributes to the rather diverse results is the method of imperfection introduction into silicon. It cannot be said with certainty that careful checks were made in some of these experiments to assure that the properties measured, such as the thermal activation energy, are indeed due to the intended impurity or defect and not due to other centers also introduced during the high temperature chemical or physical processes used to generate these defects.

In this paper, we will review some of the new experimental techniques to determine the electrical and optical properties of the electrons and holes bound at the imperfection centers. The new techniques have been extensively developed since 1965. [1,2][+] They have many advantages over the older Hall and conductivity and the optical absorption methods for studying material physics. The new methods are extremely sensitive and the experimental data can be unambiguously interpreted.

The new techniques involve the detection of electrons or holes trapped at imperfection centers in a region of a semiconductor which is depleted of free or mobile electrons and holes. [1,2] This region may be the space charge layer of a reverse biased p-n junction, a Schottky barrier or a MOS capacitor.

II. PARAMETERS CHARACTERIZING THE IMPERFECTIONS

Let us first give a brief review of the physical processes and the parameters which characterize the electron or hole generation, recombination and trapping processes at the imperfection centers. The three most important physical mechanisms

---

[+][ ]These refer to the titles given in the bibliography.

-3-
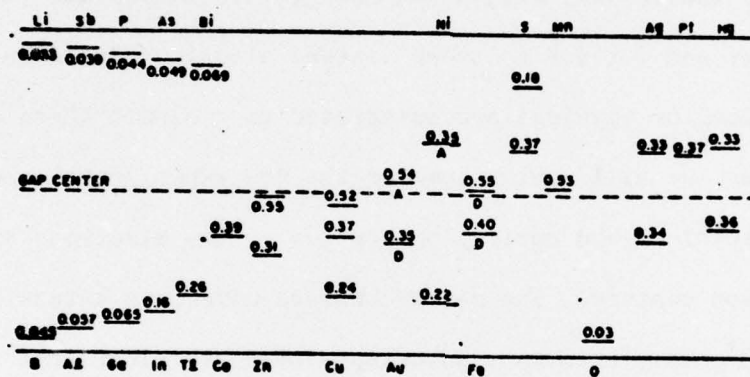
Figure 1. Experimental thermal activation energies of
electrons and holes at impurity centers in Si.
From S. M. Sze, Physics of Semiconductor Devices,
Wiley, 1969.

for energy conservation are the thermal, the optical and the Auger-Impact processes. [35] Their quantum mechanical transitions are shown in Figure 2. In the four thermal transitions of electrons and holes at the imperfection center, the phonon or lattice vibration supplies or carries away the energy during the transition. In the four optical transitions, photons provide the required energy conservation. In the eight Auger-impact transitions, an energetic electron or hole is the transition partner.

Figure 2 also gives the transition rates. The kinetic coefficients are first order, that is, the first order dependences of the bound and free particle concentrations are explicitly written out. For example, the thermal capture rate of electrons is proportional to the electron concentration, n, and to the trapped hole concentration, p_T. c_n^t is the proportionality constant or the thermal capture coefficient of electrons.

Similarly, c_n^o is the corresponding coefficient for optical capture. It is better known as the radiative capture coefficient of electrons.

Thermally averaged transition rate coefficients of the emission transitions are similarly defined. For example, e_n^t is the thermal emission rate of a bound or trapped electron to the conduction band and e_n^o is the optical emission rate of a bound electron to the conduction band. e_n^o is also commonly known as the photoionization rate of the imperfection center.

The thermal capture rates can be expressed as a product of the thermal capture cross section, σ_n^t or σ_p^t, and the thermal velocity, θ_n or θ_p, of the carrier being captured. This is illustrared in Figure 3. Similarly, the optical emission rate, e_n^o and e_p^o, can be expressed as a product of the photoionization cross section, σ_n^o and σ_p^o, and the photon flux Φ.

It has been commonly assumed that mass action law can be applied so that the ratio of the thermal emission to capture coefficients is equal to the

-5-

THERMAL   OPTICAL   AUGER-IMPACT

n

p_T n_T

p

PHONONS   PHOTONS

a b c d   a b c d   a b a b c d c d

TRANSITION RATE

a ELECTRON CAPTURE $(c_n^t + c_n^o + c_n^n n + c_n^p p)\, np_T$

b ELECTRON EMISSION $(e_n^t + e_n^o + e_n^n n + e_n^p p)\, n_T$

c HOLE CAPTURE $(c_p^t + c_p^o + c_p^p p + c_p^n n)\, pn_T$

d HOLE EMISSION $(e_p^t + e_p^o + e_p^p p + e_p^n n)\, p_T$

RATE EQ. IS $\dfrac{\partial n_T}{\partial t} = a - b - c + d$
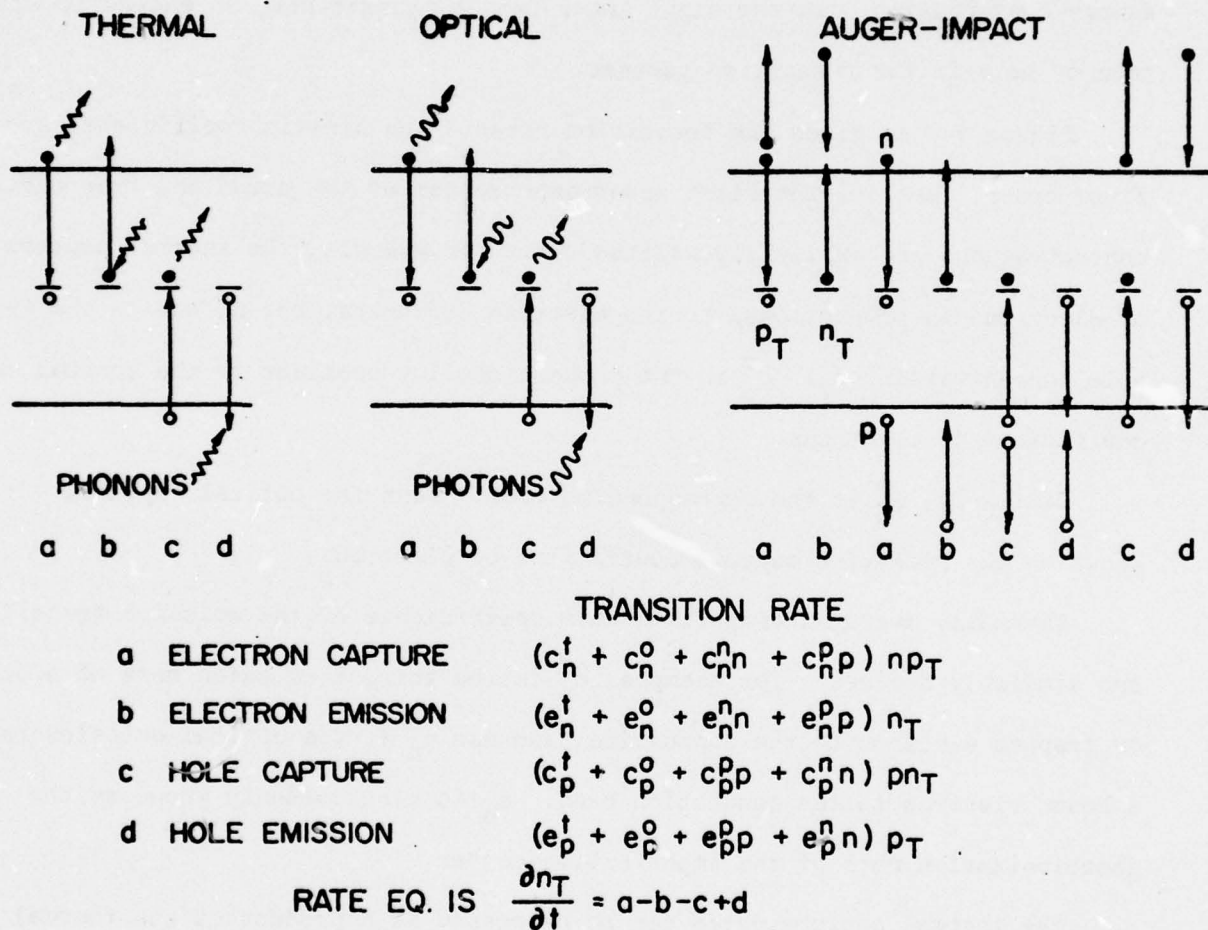
Figure 2. Electron and hole capture and emission transitions
and the transition rates of the thermal, optical and
Auger-impact processes at an impurity center. [35]

-6-

THERMAL   OPTICAL

E_C

E_T

E_V

$(a)^t$ $(b)^t$ $(c)^t$ $(d)^t$ $(b)^o$ $(d)^o$

RATES   RATES

(a) $c_n^t n p_T$ $c_n^t = \sigma_n^t \theta_n$

(b) $e_n^t n_T$ $e_n^t = \sigma_n^t \theta_n N_c e^{-(E_C-E_T)/kT}$ $e_n^o n_T$ $e_n^o = \sigma_n^o \Phi$

(c) $c_p^t p n_T$ $c_p^t = \sigma_p^t \theta_p$

(d) $e_p^t p_T$ $e_p^t = \sigma_p \theta_p N_v e^{-(E_T-E_V)/kT}$ $e_p^o p_T$ $e_p^o = \sigma_p^o \Phi$
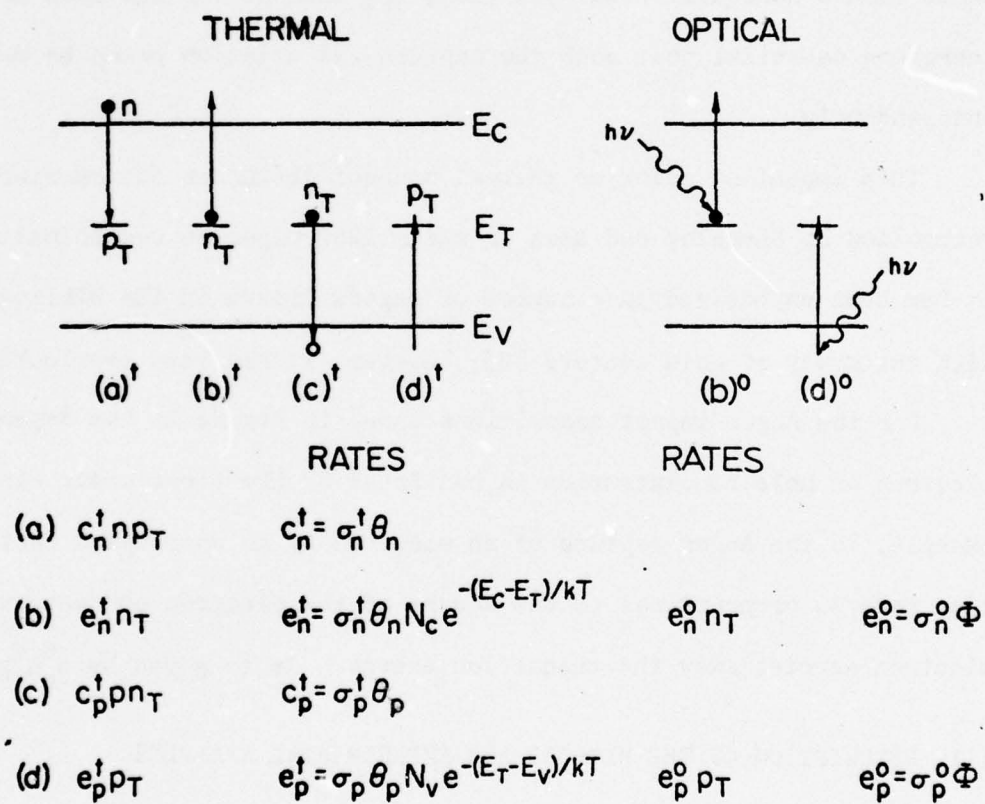
Figure 3. Thermal capture and emission cross sections and photoionization cross sections of electrons and holes at an impurity center.

equilibrium constant, $e_n/c_n = n_1$ or $e_p/c_p = p_1$. These give $\sigma_n^t = c_n/\theta_n = e_n/n_1\theta_n$ and $\sigma_p^t = c_p/\theta_p = e_p/p_1\theta_p$ which are used to calculate the capture rate and cross section from the emission rate data. Such a procedure is correct only at thermal equilibrium. Even at thermal equilibrium, it is very inaccurate since the thermal emission rate is strongly temperature dependent and has a large thermal activation energy as indicated by $e_n^t = c_n^t N_C \exp[-(E_C - E_T)/kT]$ for electrons in Figure 3.

In practical situations and in our experiments performed in a depletion region, a high electric field may exist to give appreciable hot electron (or hole) effects. Under such a nonequilibrium condition, the mass action law does not hold. It is therefore essential that both the capture and emission rates be measured independently.

This important point on thermal nonequilibrium or hot carrier effect was recognized by Shockley and Read in their 1952 paper on recombination kinetics. It has been emphasized in a number of papers listed in the bibliograph, beginning with the study of gold centers [3]; however, it has been overlooked frequently.

For the Auger-impact transitions shown in Figure 2, the dependences on the electron or hole concentration is nonlinear in the first order kinetics. For example, in the Auger capture of an electron by an unoccupied center, the transition rate is proportional to the square of the electron concentration if another electron carries away the transition energy. It is given by $c_n^n n^2 p_T$ in Figure 2.

III. DESCRIPTION OF THE METHODS AND EXPERIMENTAL EXAMPLES

The new methods [7] of measuring these capture and emission rate coefficients are suggested from the rate equations in Figure 2 which can be simplified to

$$\frac{dn_T}{dt} = -(c_n n + e_n + c_p p + e_p)n_T + (c_n n + e_p)N_{TT} \qquad (1)$$

where use is made of $p_T + n_T = N_{TT}$. N_{TT} is the concentration of the centers. The kinetic coefficients are defined by:

-8-

$$c_n = c_n^t + c_n^o + c_n^n n + c_n^p p ,$$

$$c_p = c_p^t + c_p^o + c_p^p p + c_p^n n ,$$

$$e_n = e_n^t + e_n^o + e_n^n n + e_n^p p ,$$

and

$$e_p = e_p^t + e_p^o + e_p^p p + e_p^n n .$$

(2)

It is obvious that linearization of the rate equation is achieved if the electron and hole concentrations are zero or *constant*. This immediately suggests the use of the depleted region of a p-n junction, a Schottky barrier or a MOS capacitor where the electron and hole concentrations are zero.

The linear system is the most accurate system for measuring the fundamental kinetic parameters, since any perturbations applied to the system will decay exponentially with time. In fact, the reciprocal of the decay time constant is equal to the sum of all the emission and capture rates as indicated by Equations (1) and (2). The time constant is given by

$$\tau = \frac{1}{c_n n + e_n + c_p p + e_p}$$

(3)

One very important and unique feature of a depleted region is that the decay time constant is independent of the concentration of the imperfection centers. This avoids the uncertainty and error which occur in small-signal photoconductivity experiments whose decay time constant depends on the concentration of the imperfection centers. It also avoids the difficulty of defining a time constant in large-signal nonlinear photoconductivity experiments where the decay is not exponential.

Another unique feature is the true exponential decay predicted from the simple model. It allows us to accurately study the physical factors which give rise to a distribtuion of time constants. For example, there are substantial hot-electron or hot-hole effects in a reverse biased p-n junction which give

-9-

rise to electric field dependences of the thermal capture and thermal emission rate coefficients.

The most important feature is the fact that the measurements can be performed in a device structure which has been subjected to high temperature processes such as a diffused p-n junction or transistor. However, the measurements can also be made on original and not-heat-treated samples using a Schottky barrier or MOS structure with anodized oxide.

Let us now proceed to describe the experiments. We can observe two types of transients from the emission of trapped electrons or holes in a depleted region after a perturbation is applied. [7] One is the current transient and the other is the small-signal high-frequency capacitance transients. These are illustrated in Figure 4 for a p-n junction. The applied voltage sequence is as follows. The junction is initially zero biased. This is the perturbation which sets the initial charge condition of the traps. As indicated in the upper energy band diagram, this initial condition is that the traps on the n-type side of the junction are filled with electrons. Next, a negative voltage is applied to reverse bias the p-n junction and to create a depleted space charge region. Immediately after the voltage is switched to a reverse bias, the electrons near the junction are swept out of the junction region in a few transit times, about 10^{-12} seconds or a few picoseconds. The beginning of this sweep-out process is shown in Figure 4(b) and the end is shown in Figure 4(c). At the end of the sweep-out period, which lasts for a few picoseconds, a depletion region is created. During this very short sweep-out period, the trapped electrons are still all trapped at the imperfection centers.

These trapped electrons are slowly excited out of the imperfection centers either thermally, or optically or by impact after the reverse bias voltage is applied. The energy band diagram in Figure 4(c) shows that the trapped electrons are released and then swept out to the n-type region, producing an electron current, i_c. Simultaneously, the trapped holes are created which are also thermally excited into the valence band and then swept out to the p-type region

-10-
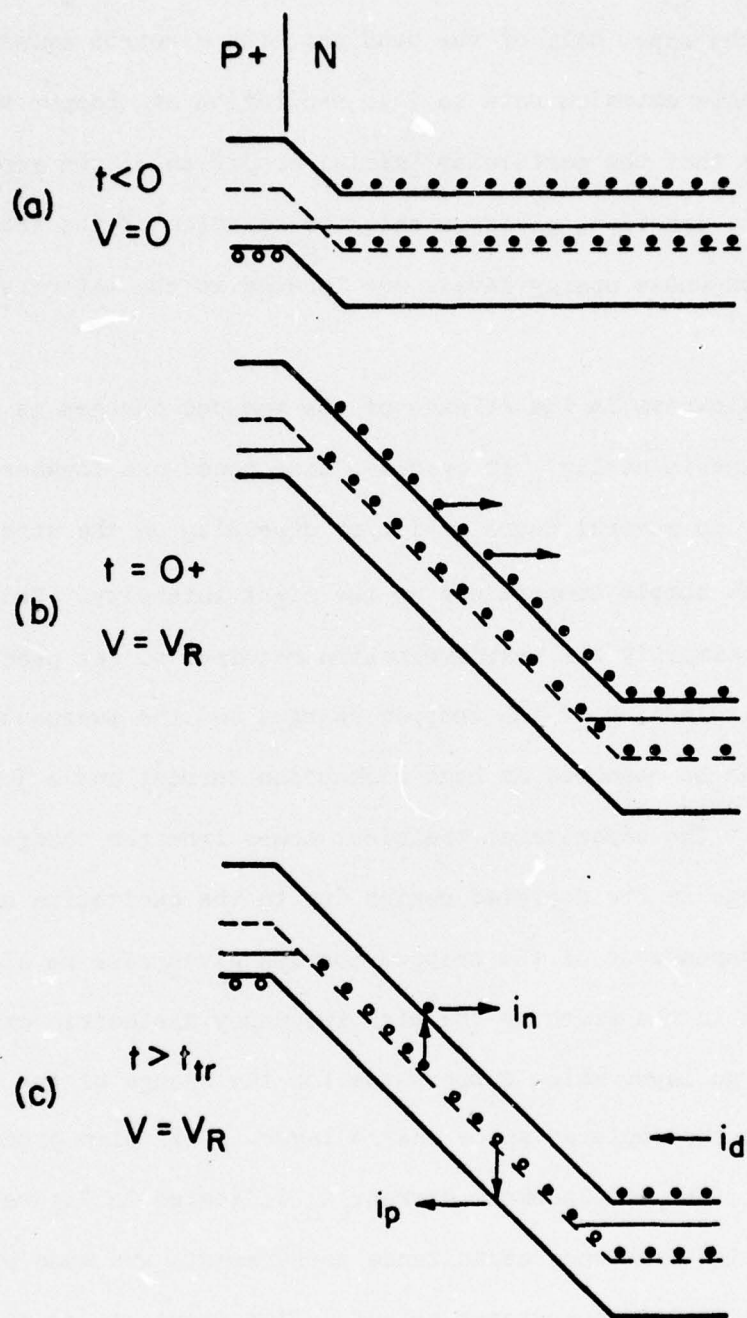
Figure 4. Emission of trapped electrons and holes at an imperfection center in the depleted space charge region of a reverse-biased p-n junction.

by the high electric field, producing a hole current i_p. Generally, for an energy level in the upper half of the band gap, the electron emission rate is much higher than the hole emission rate so that excitation of trapped holes can be neglected. This means that the particular initial condition of the traps, set by zero biasing the junction, gives us only the kinetics of the trapped *majority* carriers at those traps whose energy levels are located in the majority carrier half of the band gap.

The slowness in the release of the trapped charges is what makes it easy to observe experimentally. It involves time constants anywhere from a few milliseconds or shorter to several hours or longer depending on the strength of the excitation such as the sample temperature or the light intensity. The relatively long time constants simplify the instrumentation required to get precise data.

The excitation of the trapped charges and the sweep-out of the released charges can be observed as both a junction current and a junction capacitance transient. The capacitance transient comes from the change of the trapped space charge in the depleted region due to the excitation and sweep-out processes. The time dependence of the trapped charges gives rise to a corresponding time dependence in the width or the high frequency dielectric capacitance of the space charge layer which compensates for the change of the total trapped charges in the depleted space charge layer. This also produces the third component of current, the displacement current i_d indicated in Figure 4(c).

The high frequency capacitance measurements are made at one Mega Hertz using commercial analog capacitance meters. Time constants as small as one millisecond can be accurately determined. The capacitance measurement is more convenient for larger time constants at lower temperatures. On the other hand, the current transient has large magnitude only at high temperatures when the thermal emission rates are high and the time constants are small. Consequently, the two measurements

-12-

compliment each other. The combined current and capacitance transient measurements can give time constant data over ten orders of magnitude, to be illustrated later.

Let us now go through a simple analysis of the capacitance transient using Figure 5. Here, a more realistic view of the potential energy variation with position is shown. Consider first the space charge distribution versus position. Since a constant voltage is applied to the junction, the change of the trapped electron and hole charge concentrations, indicated by the shaded area labeled n_T, must be compensated by the bulk electrons moving into the edge region of depletion layer, given by the shaded area at the edge. The flow of the bulk electrons into the edge region then reduces the width of the depleted layer. The decrease of the depletion layer width is detected as an increase of the high-frequency dielectric capacitance of the depleted layer.

A simple one-dimensional parallel plate capacitance calculation is given below for a gold doped p+/n diffused or Al/n Schottky diode. The electron charge induced at the edge layer, Ndw, is given by

$$Ndw = (N_{DD}-N_{Au})dw = \int_0^W n_T(w,t) \frac{x}{w} dx = n_T(t) \frac{w}{2} \tag{4}$$

where N_{Au} is assumed to be indepedent of position. The fractional change of the space charge capacitance with time is then given by

$$\frac{\Delta C(t)}{C_\infty} = \frac{dw}{w} = \frac{n_T(t)}{2(N_{DD}-N_{Au})} . \tag{5}$$

Here $n_T(t)$ is obtained from the solution of Equation (1) using the depletion approximation, N=P=0, and is given by

$$n_T(t) = N_{Au} e^{-t/\tau} \tag{6}$$

where

$$\tau = 1/(e_n^t + e_p^t) \simeq 1/e_n^t \qquad \text{if } e_n^t \gg e_p^t . \tag{7}$$

The total capacitance change during the entire transient is then given by

$$\frac{\Delta C(t=\infty)}{C_\infty} = \frac{N_{Au}}{2(N_{DD}-N_{Au})} \simeq \frac{N_{Au}}{2N_{DD}} \qquad \text{if } \Delta C(\infty) \ll C_\infty . \tag{8}$$

Thus, the capacitance transient data gives both the electron emission rate, e_n^t, and the gold concentration, N_{Au}. The approximation indicated in Equation (8)
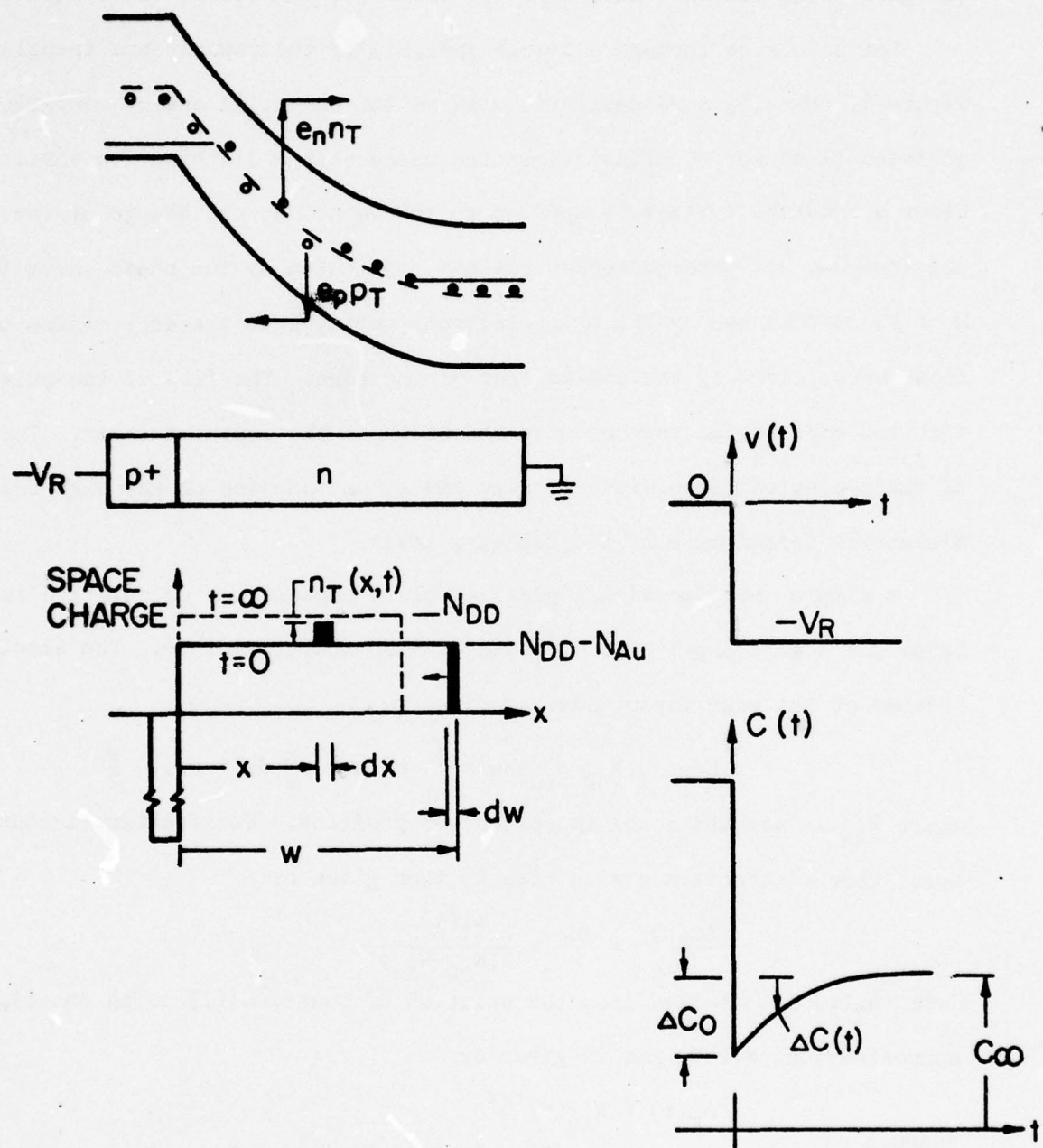
Figure 5. The space charge distribution for a simple quantitative analysis of the capacitance transient.

P+ | N

(a) t<0
    V=0

(b) t = 0+
    V = V_R

(c) t > t_tr
    V = V_R
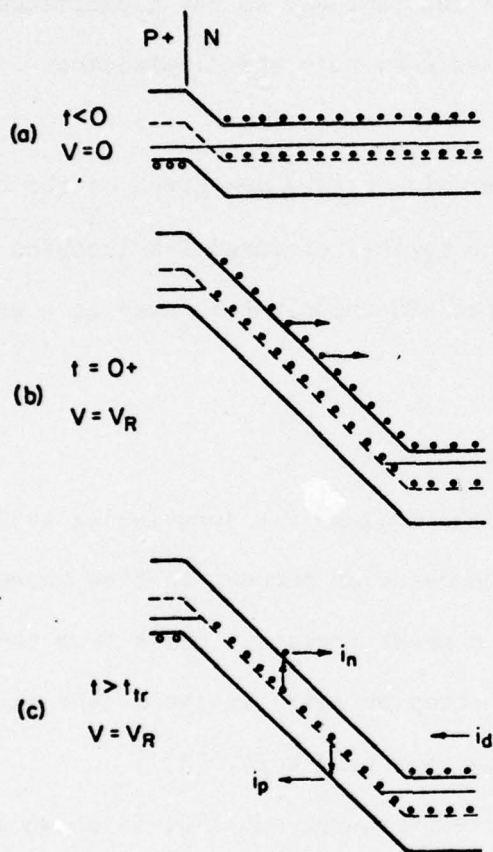
$$-\frac{dn_T}{dt} = (e_n^t + e_p^t)n_T - e_p^t N_{TT}$$

$$n_T(t) = N_{TT}\left[\frac{e_p^t}{e_n^t + e_p^t} + \frac{e_n^t}{e_n^t + e_p^t}\exp(-t/\tau)\right]$$

$$\tau = \frac{1}{e_n^t + e_p^t}$$

$$i(t) = \left(\frac{qwA}{2}\right)\left(e_p^t p_T + e_n^t n_T\right)$$

$$C^2(t) = \frac{qA^2}{2K_S\epsilon_o}(V_D + V_R)(N_{DD} - n_T)$$

A = JUNCTION AREA

i_n i_d i_p

Figure 6.   A summary of the expressions for the capacitance and
current transients in a reverse-biased p-n junction for
spatially constant trapping center concentration.

-15-

shows that the interpretation is the simplest if the concentration of the imperfection center, N_{Au}, is much smaller than the concentration of the majority doping impurity, N_{DD}.

A summary of the equations for the capacitance and current transients are shown in Figure 6 for spatially constant concentrations of shallow impurities and generation-recombination-trapping centers. The formula for the current transient indicated here can be derived in the same way as the capacitance transient formula just given, by adding the electron, hole and displacement currents. [7]

Some examples of the results of our studies [1-34] are given on the next few figures. The cross sectional view of a typical diffused P+N junction on silicon is shown in Figure 7. A ring shaped MOS capacitor is used as a guard ring to cut off any surface channel.

3.1 Examples Using the Thermal Emission Processes

The current transient of a gold-diffused silicon P+N junction at 44°C [7] is shown in Figure 8. Note the linear dependence of current on time shown on the semilog scale in the lower diagram. This current transient comes from the thermal emission of electrons trapped at the gold acceptor level in the n-type silicon which is located at 570 meV below the conduction band edge. [3]

The capacitance transient at a lower temperature, -65.1°C, is shown in Figure 9. Note again the linear decay on the semilog plot, indicating a single time constant.

The electric field dependence of the thermal emission rate of trapped electrons at the gold acceptor is shown in Figure 10 from capacitance transient measurements at seven temperatures. [9] The electric field is increased by increasing the reverse bias voltage. This dependence suggests a Poole-Frenkel impurity potential barrier lowering effect which enhances the emission rate.

-16-
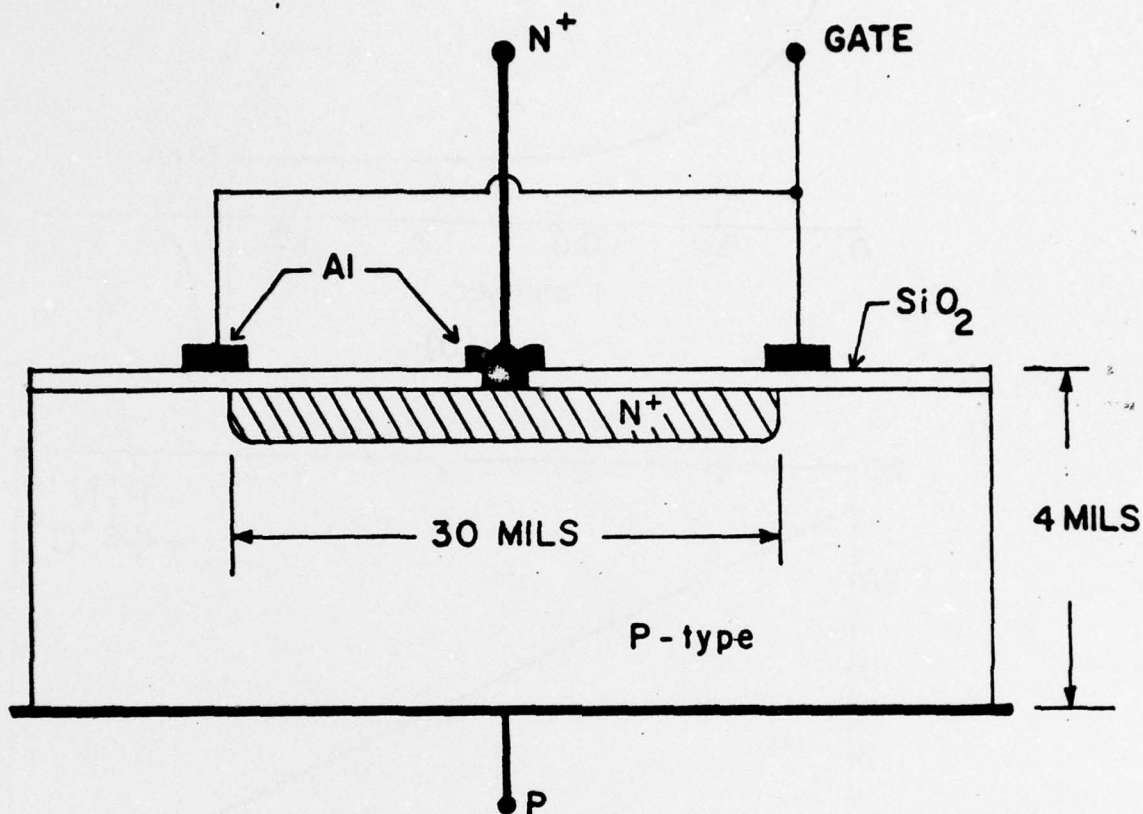
VERTICAL SCALE EXPANDED

Figure 7.   The cross sectional view of a diffused n+p silicon
junction with a MOS capacitance guard ring to cut off
the surface channels.

-17-
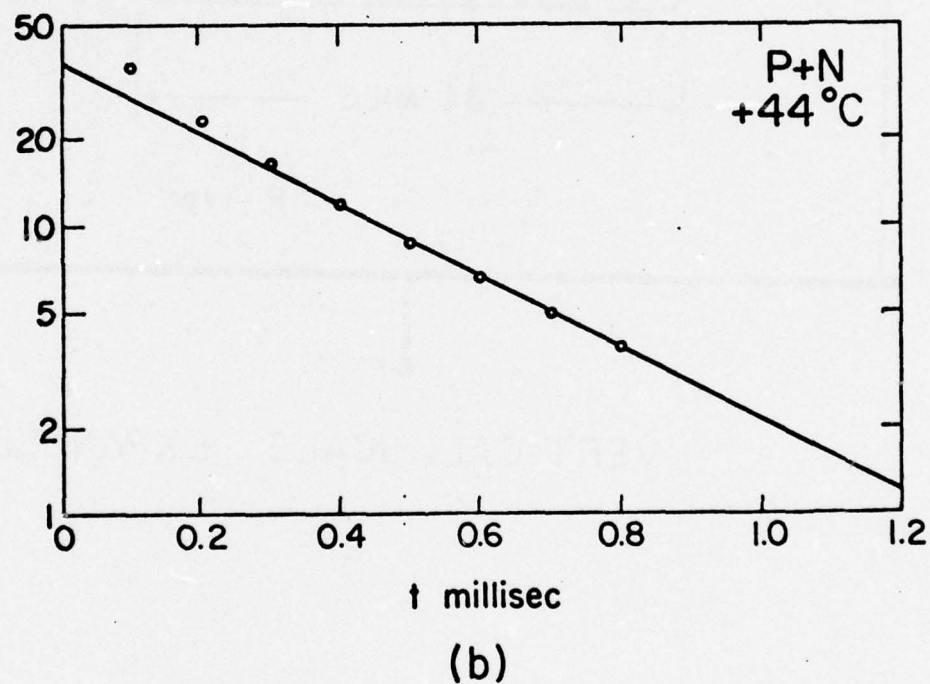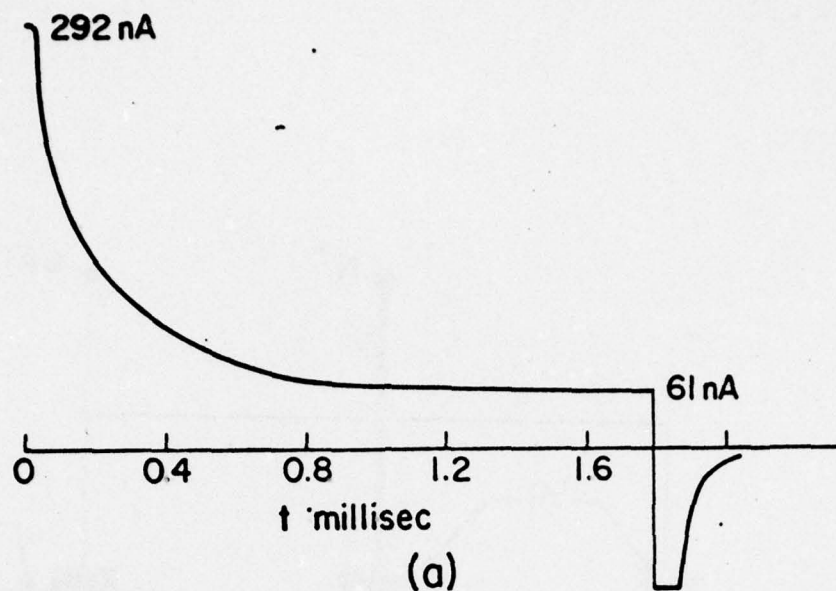
Figure 8. An example of the experimentally observed junction current
transient in a gold-doped silicon p+n junction at 44°C.
Note the nearly exponential decay. [7]

-18-
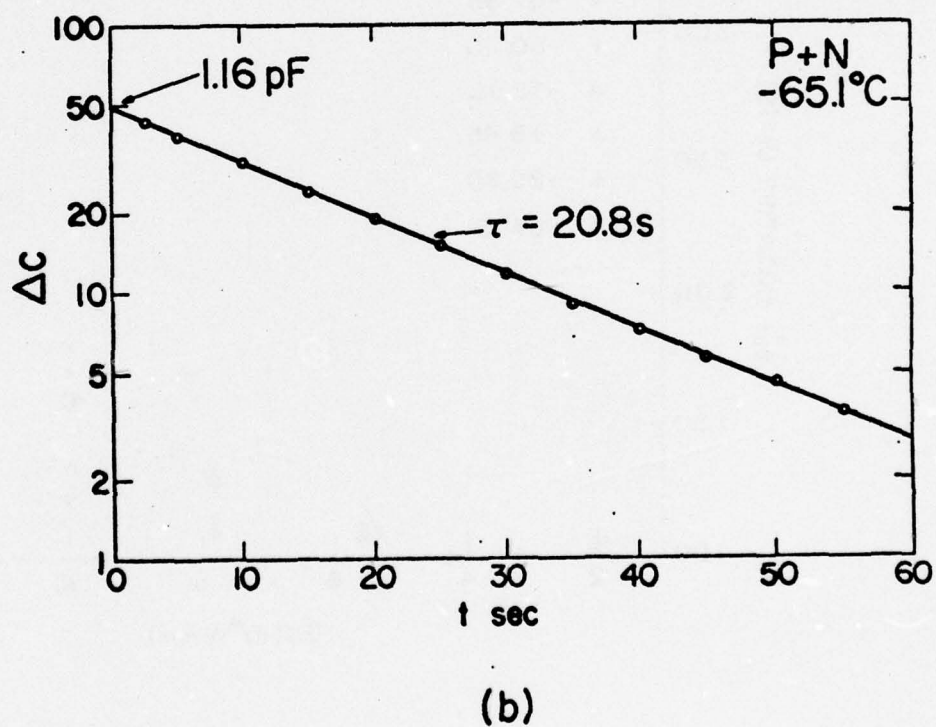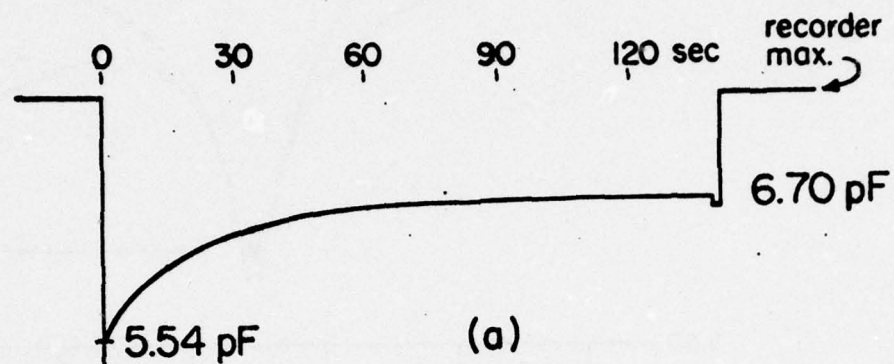
Figure 9. An example of the experimentally observed junction capaci-
tance transient in a gold-doped silicon p+n junction at
-65.1°C. Note the nearly exponential decay. [7]

-19-
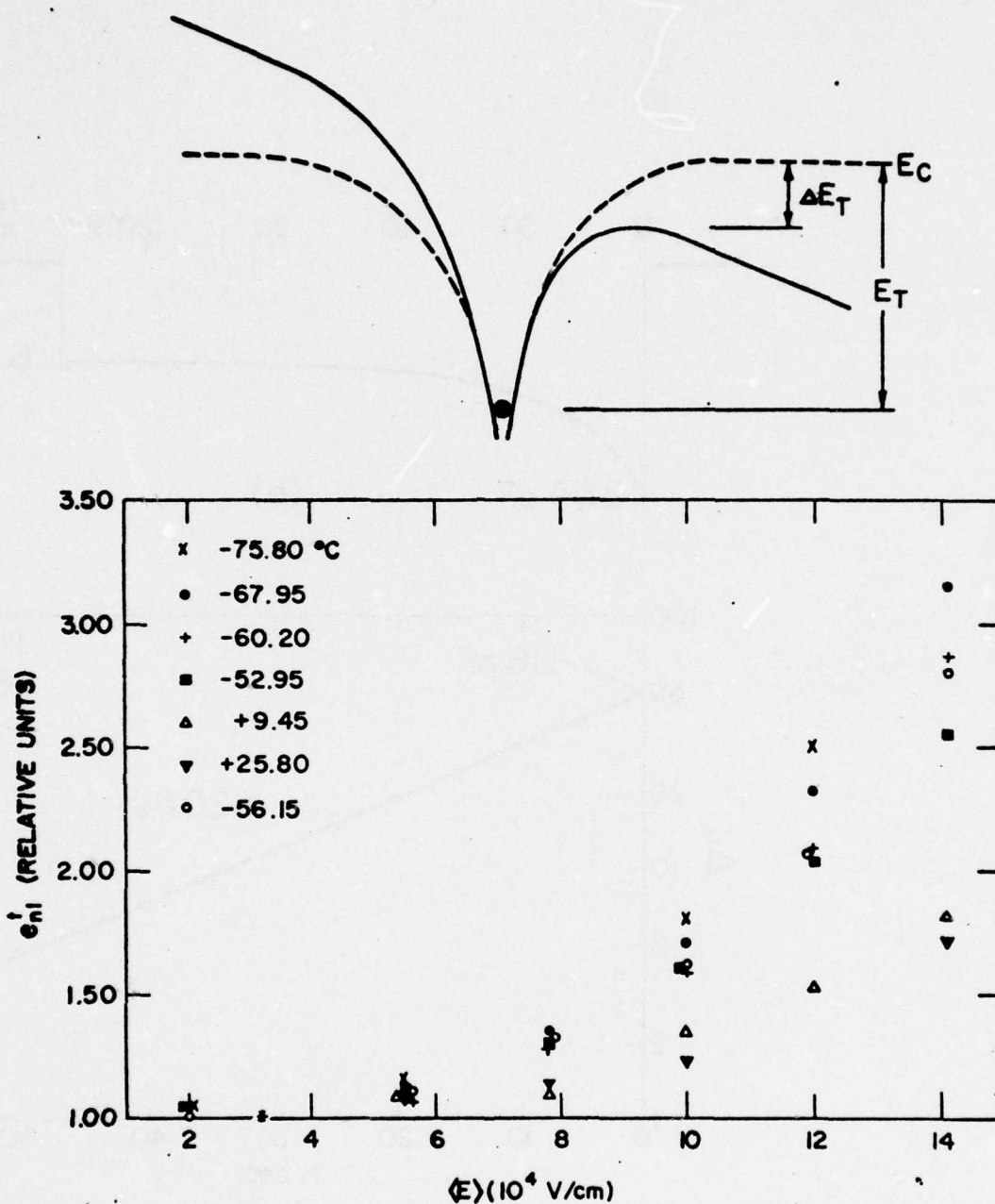
Figure 10. An example of the observed electric field dependence of the thermal emission rate of electrons trapped at the gold acceptor level in silicon.

The observed temperature dependence is consistent with the simple equation from barrier lowering given by $e_n = e_n(0)\exp(\Delta E_T/kT)$. However, a quantitative comparison between the theory and experiments has not been successful.

The next figure, Figure 11, shows the thermal emission rate of electrons or holes trapped at the gold acceptor or donor centers in silicon at low electric fields. [3] Low temperature data are from capacitance transients while high temperature data are from current transients. About 10 decades of data are obtained. The slope of the three lines gives the three thermal activation energies which are indicated in the corresponding energy level and transition diagrams.

Applications of the capacitance transient method are shown in the next four figures. Figure 12 shows the spatial variations of the phosphorus donor density, N_D, in a boron diffused P+N control diode and the deep level zinc acceptor density, N_{Zn}, in a boron as well as zinc diffused P+N junction. [25] Note the rise of the zinc concentration towards the boron diffused P+ region, suggesting an increase of the zinc solubility in the silicon surface region which is diffused with a high concentration of boron.

Figure 13 shows a plot of the concentration of a shallow zinc-boron complex center versus the zinc concentration. [25] The concentrations are obtained from capacitance data on three N+P phosphorus as well as zinc diffused silicon diodes. The dependence suggests that the complex is a compound of three zinc atoms surrounding one boron atoms.

Figure 14 shows the concentration of the A-center or the Oxygen-Vacancy pair in a high temperature processed float-zone silicon after it is bombarded by one-MeV electrons. [30] The initial oxygen concentration is negligible. The vacancy is uniformly generated by a one-MeV electron beam. The constancy of the Oxygen-Vacancy concentration with position suggests that oxygen is diffused into

-21-
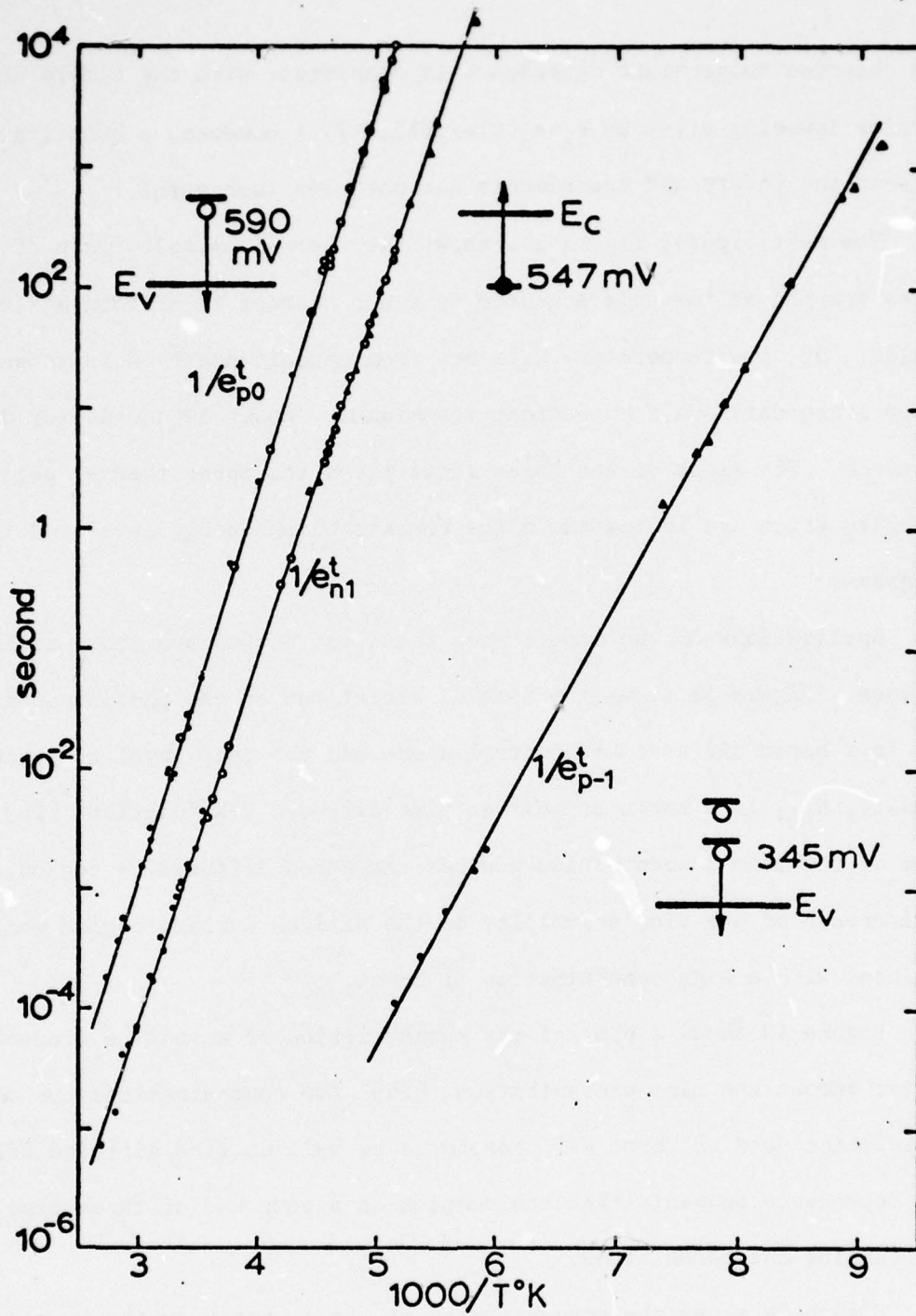
Figure 11. The reciprocal thermal emission rate of electrons and holes from the gold acceptor and donor centers in silicon at low electric fields obtained from the current and capacitance transient decay time constant measurements.
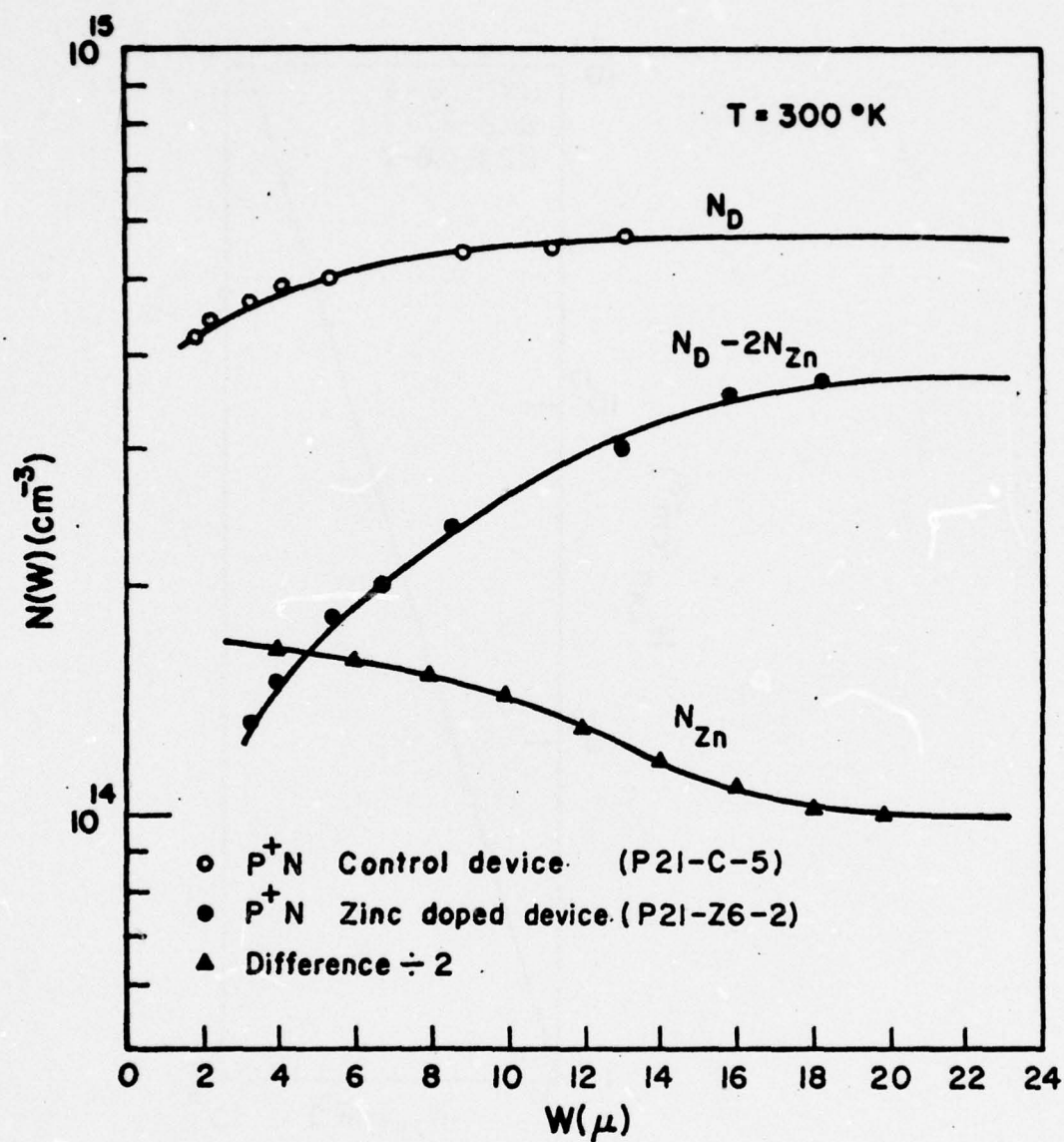
Figure 12. An application of the capacitance transient. The spatial distributions of the phosphorus donor and zinc acceptor impurities in boron diffused silicon p+n junctions are obtained from the total change of the capacitance transients in a range of reverse bias voltages. [31]

-23-

10^{14}
B21-Z6-2
B22-Z7-7
B23-Z8-7

N_{ZnB} (cm^{-3})

10^{13}

10^{12}

10^{11}

10^{14} N_{Zn}(cm^{-3}) 10^{15}
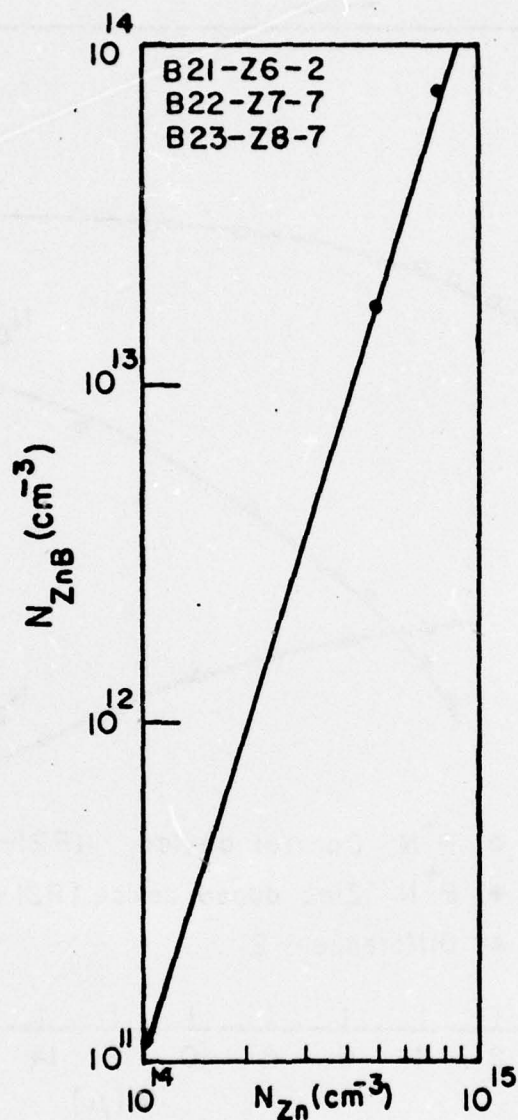
Figure 13.   An application of the total change of the capacitance
transient showing the concentration of the Zn-boron
complex center as a function of zinc concentration.
The cubic power dependence of N_{ZnB} on N_{Zn} suggests that
the complex is a Au_3B compound. [31]

-24-
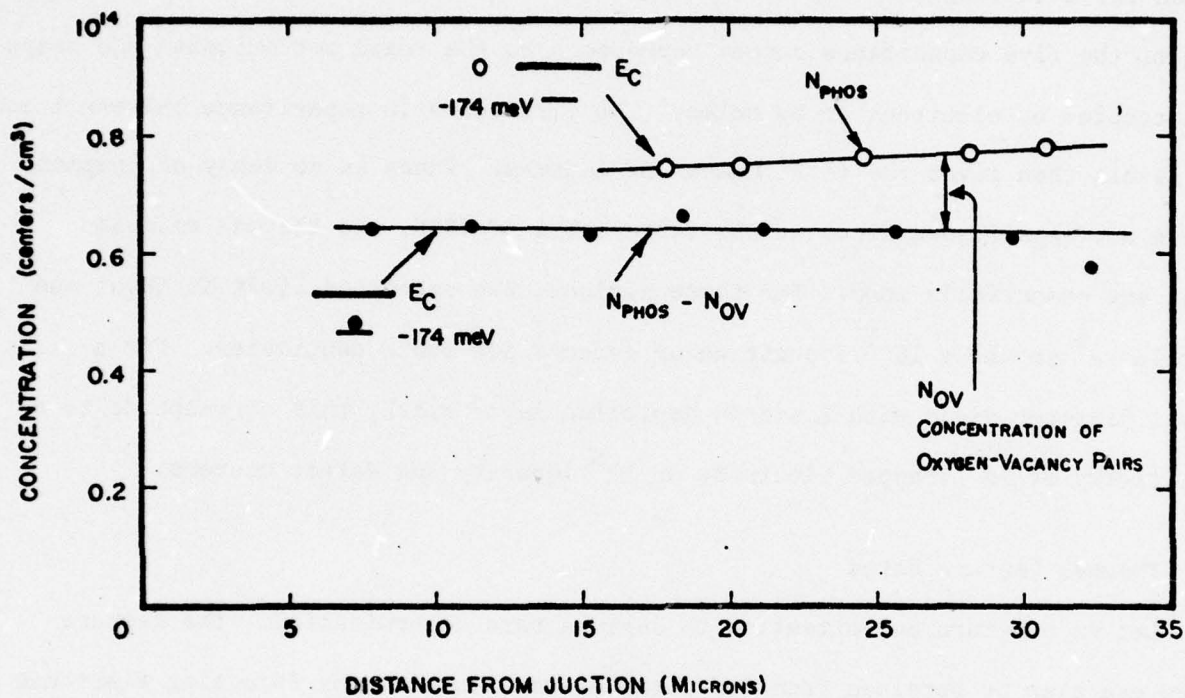
Figure 14. An application of the total change of the capacitance transient showing spatial variation of the concentration of the A-center or the vacancy-oxygen pair after the vacancies are generated uniformly by one MeV electron irradiation. [30]

silicon during the high temperature processing to a depth of more than 30 microns. Aluminum Schottky barrier diodes, evaporated onto the surface of the n-type float-zone silicon without heat treatment, showed less than 10^{11} oxygen-vacancy pairs per cubic centimeter after one-MeV electron irradiation.

Figure 15 illustrates the sensitivity of the dark capacitance transient method for detecting the deep level impurities. [4] The two capacitance levels of each of the five capacitance curves correspond to the traps not occupied and traps all occupied by electrons or by holes. The difference in capacitance between these two levels then gives the total number of centers. There is no decay of trapped charge nor capacitance since at the temperature of 77°K, the thermal emission rates are essentially zero. For these devices, the detection limit is about one part in 10^4 or about 10^{11} impurities or defects per cubic centimeter. For a 30 mil diameter diode with 2 micron depletion layer width, this corresponds to a sensitivity of 10^5 trapped electrons or 10^5 impurity and defect centers.

3.2 Thermal Capture Rates

Let us now turn our attention to capture rate determination. The capture rates can also be obtained from capacitance transient data by injecting electrons or holes into the depletion region. [9,7] Figure 16 illustrates two methods of measuring the capture rate, by getting the same initial charge state of the traps in two ways. In the middle energy band diagram, the trapped electrons are excited out of the traps either thermally or by exposure to an extrinsic light. After the traps are emptied, the semiconductor surface is exposed to an intrinsic light to generate electron-hole pairs at the surface. Because of the large intrinsic absorption coefficient, there is essentially no penetration of the intrinsic light into the depletion layer to cause photoexcitation of the trapped holes and electrons. The photogenerated electrons at the surface are swept into the depletion region and some of them are captured by the empty traps to give a
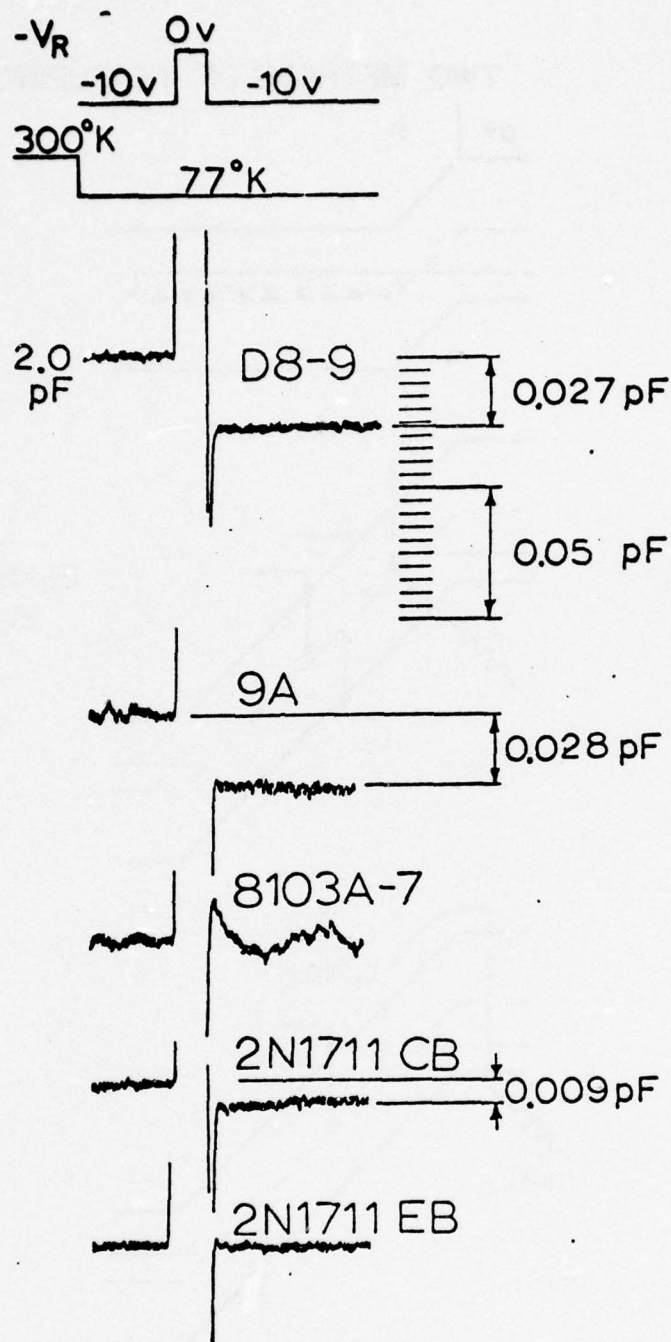
Figure 15. An application of the total capacitance change showing the concentration of majority carrier traps and recombination centers in several diodes and transistor emitter and collector junctions. The detection sensitivity limit is about 1 part in 10^4 or 10^{11} impurity atoms or traps/cm^3. [4]

TWO METHODS OF MEASURING CAPTURE RATE

p^+ n

$v(t)$

O t

$-V_R$

LIGHT FLUX

$h\nu > E_G$

$E_G > h\nu >$
$E_C - E_T$

t

C

ELECTRON
CAPTURE

$c_n N p_T$

$e_n n_T$

τ

$h\nu > E_G$

t

$$\tau = \frac{1}{c_n N + e_n}$$

$$N = I / q \theta_n A$$
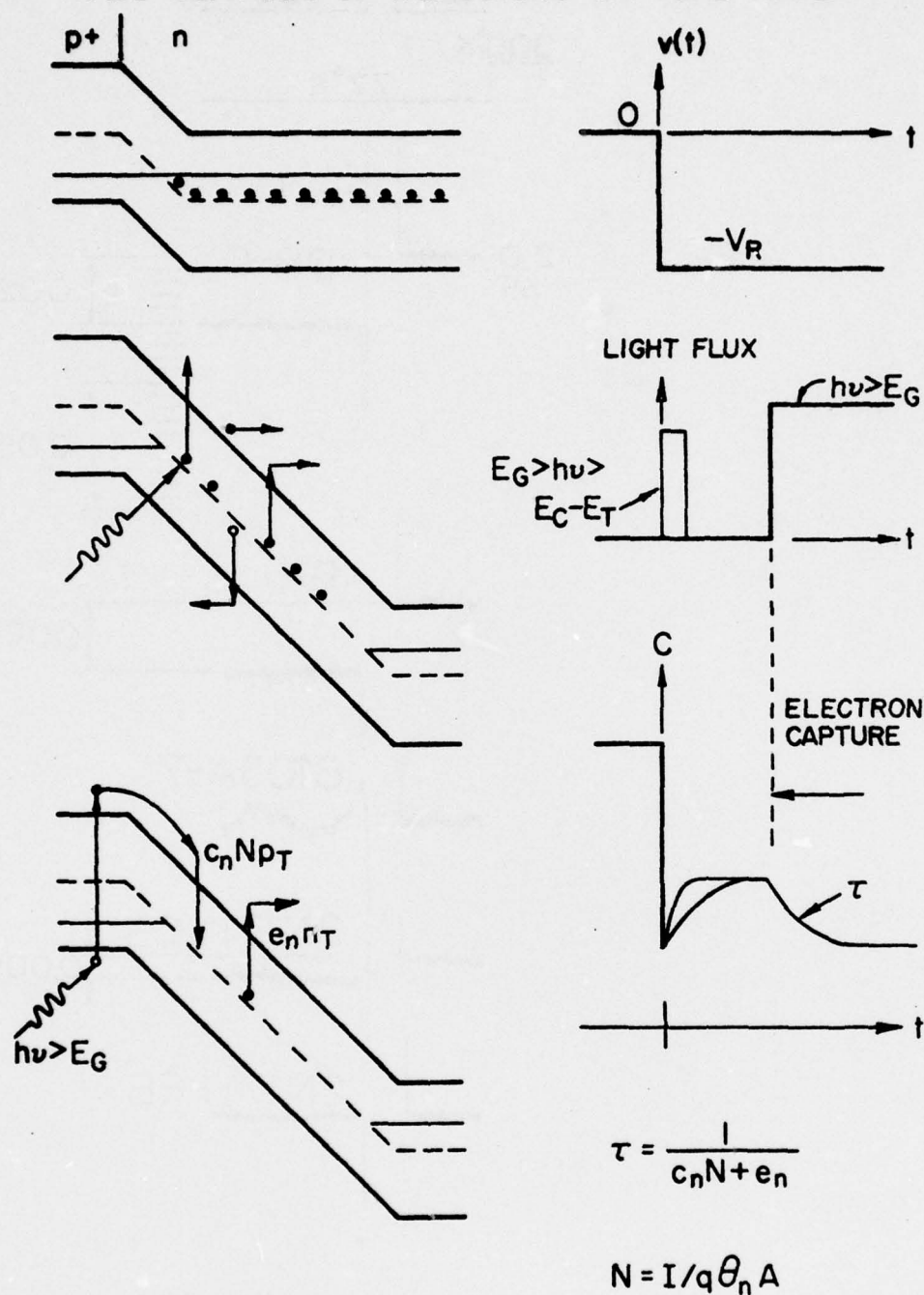
Figure 16.   The energy band diagrams, the capacitance, and the light
flux waveforms illustrating two methods of measuring the
rate of electron capture into an imperfection center in
the junction depletion region.

capacitance transient. The time constant is the reciprocal of the sum of the electron capture and emission rates as shown in Figure 16. The electron concentration in the electron capture rate is calculated from the total junction photocurrent. Both the electron concentration and the photocurrent are constant since a very small fraction of the injected electrons are captured.

Examples of the capacitance decay due to electron captured into the gold acceptor level in silicon are shown in Figure 17 for three photocurrents. [7] It is obvious that the decay rate increases with increasing photocurrent as expected from the time constant $\tau = \dfrac{1}{c_n N + e_n}$ where $N = I/q\theta_n A$, I is the photocurrent, θ_n is the electron velocity and A is the junction area.

Another example showing hole capture into both the gold donor and the gold acceptor levels in a gold diffused junction on p-type silicon [7] is given in Figure 18. Note that two exponential decays are superimposed onto each other. The faster decay is from holes captured into the gold acceptor level and the slower one is from holes captured into the gold donor level.

3.3 Impact Emission Rates

A method [9] can be developed to measure the impact ionization rate [35] at low temperatures when the thermal emission rate is negligible. This is illustrated in Figure 19. The electrons are again photogenerated on the surface and are swept into the depletion region to cause impact emission of trapped electrons. Alternatively, a forward biased emitter junction can be used to inject the electrons. [9] In contrast to the electron capture experiment just described, the traps here are initially occupied by electrons. Some of these trapped electrons are knocked out by the photogenerated and injected electrons which had gained sufficient kinetic energy in the electric field. The impact release of trapped electrons gives a capacitance transient whose time constant gives the
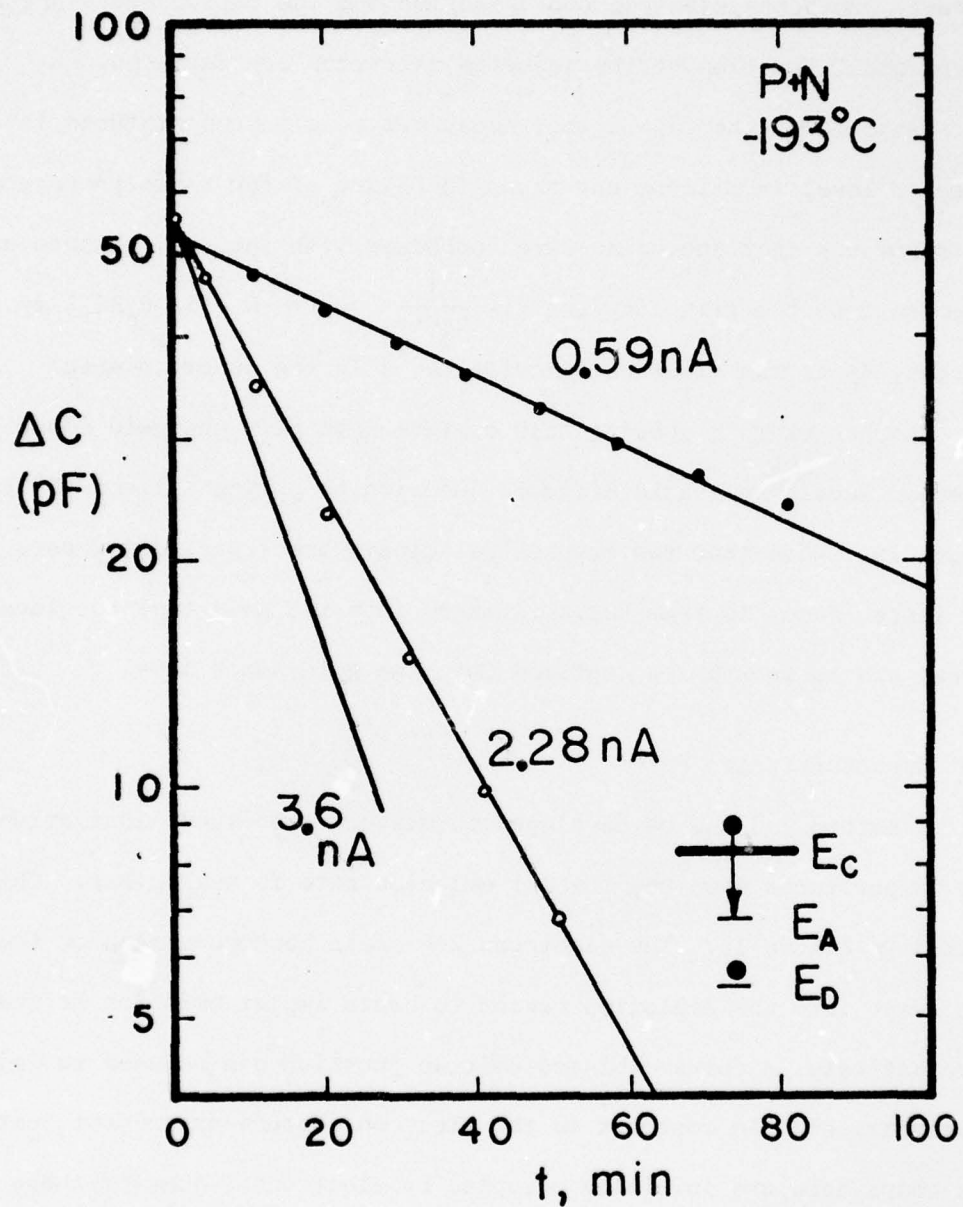
Figure 17. Experimental data illustrating the capacitance decay time constants as a function of the junction d.c. current or light intensity, due to electron capture into the gold acceptor center in a silicon p+n junction at −193°C. [7]
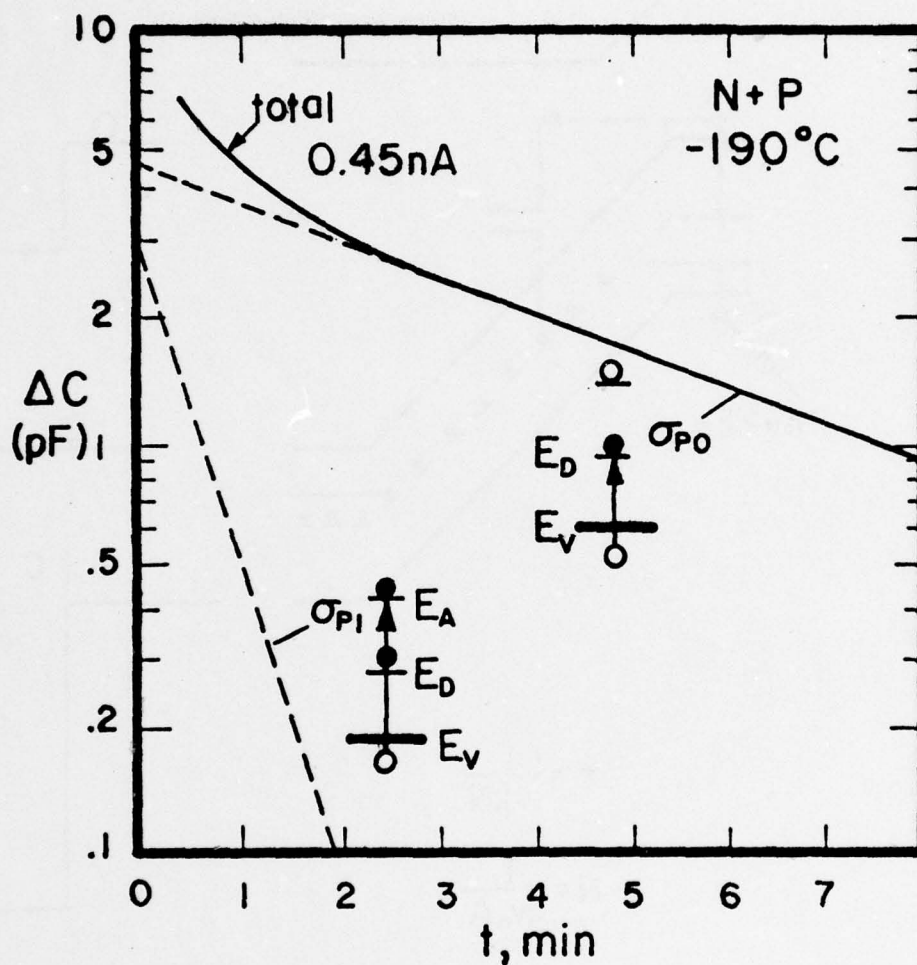
Figure 18. Experimental data illustrating the capture of holes into the gold donor and the gold acceptor levels in the p-type silicon of an n+p junction at −190°C. The data shows that there are two exponential decays in the capacitance transient due to the capture at the two gold energy levels. [7]

-31-

Figure 19. The energy band diagrams and the capacitance transient waveform illustrating a method of measuring the impact emission of trapped electrons by energetic electrons.

reciprocal impact emission rate e_n^n. Usually, we also have to take into account the recapture of the electrons which are impact released. The capture process will modify the formula given here slightly by adding a capture rate $c_n N$ to e_n^n in the time constant and by reducing the total ΔC by a factor $e_n^n/(c_n N + e_n^n)$.

Experimental data of the electric field dependence of the electron impact emission rate of trapped electrons at the double donor sulfur centers in the neutral charge state are shown in Figure 20. The general rise of the impact emission rate with increasing electric field is expected but a theory has not been worked out to account for the detailed shape.

3.4 Optical Emission Rate and Photoionization Cross Sections

Let us now move on to the determination of the photoionization cross sections or the optical emission rates of trapped electrons and holes. [7] These rate constants can again be obtained from the junction capcitance or current transients after the junction is exposed to extrinsic light at such a low temperature that the thermal emission rates can be neglected. This is illustrated in Figure 21. The capacitance transient time constant gives the photoionization rate and cross section and the total capacitance change gives the trap concentration. Because of the extremely high sensitivity of the capacitance measurement techniques, photoionization cross sections of 10^{-19} cm^2 can be measured. This corresponds to an absorption ocefficient of 10^{-3} cm^{-1} which is three orders of magnitude more sensitive than the conventional absorption measurements.

The photocapacitance transient measurements can be used to determine the photoionization threshold energies of the trapped electrons and holes. This gives another way of determining the energy levels of the bound states. It can also be used to determine whether the two energy levels belong to the same center. In Figure 22, the energy band diagram is used to illustrate the use of two extrinsic monochromatic light sources to photoionize the two sulfur donor
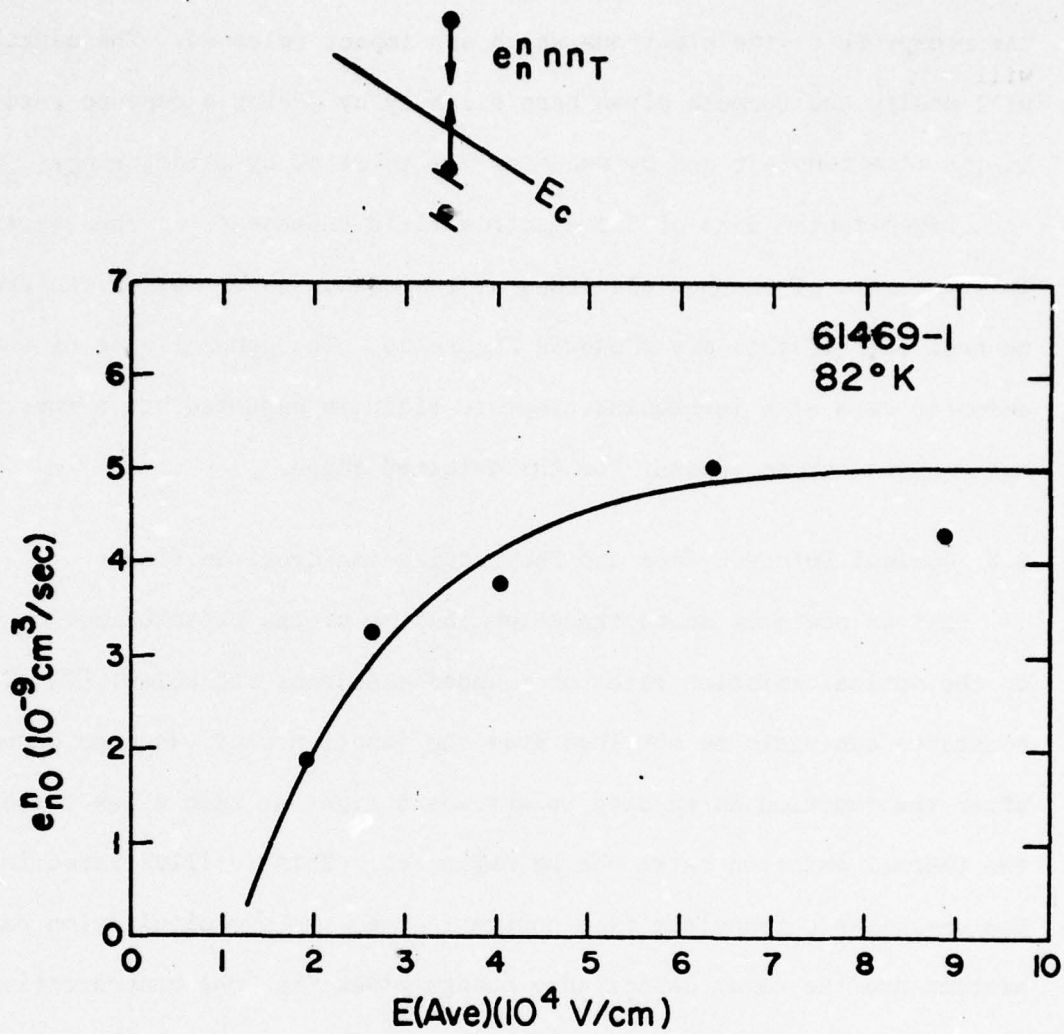
Figure 20. The observed electric field dependence of the electron impace emission rate of trapped electrons at the neutral sulfur donor center in silicon. [9]
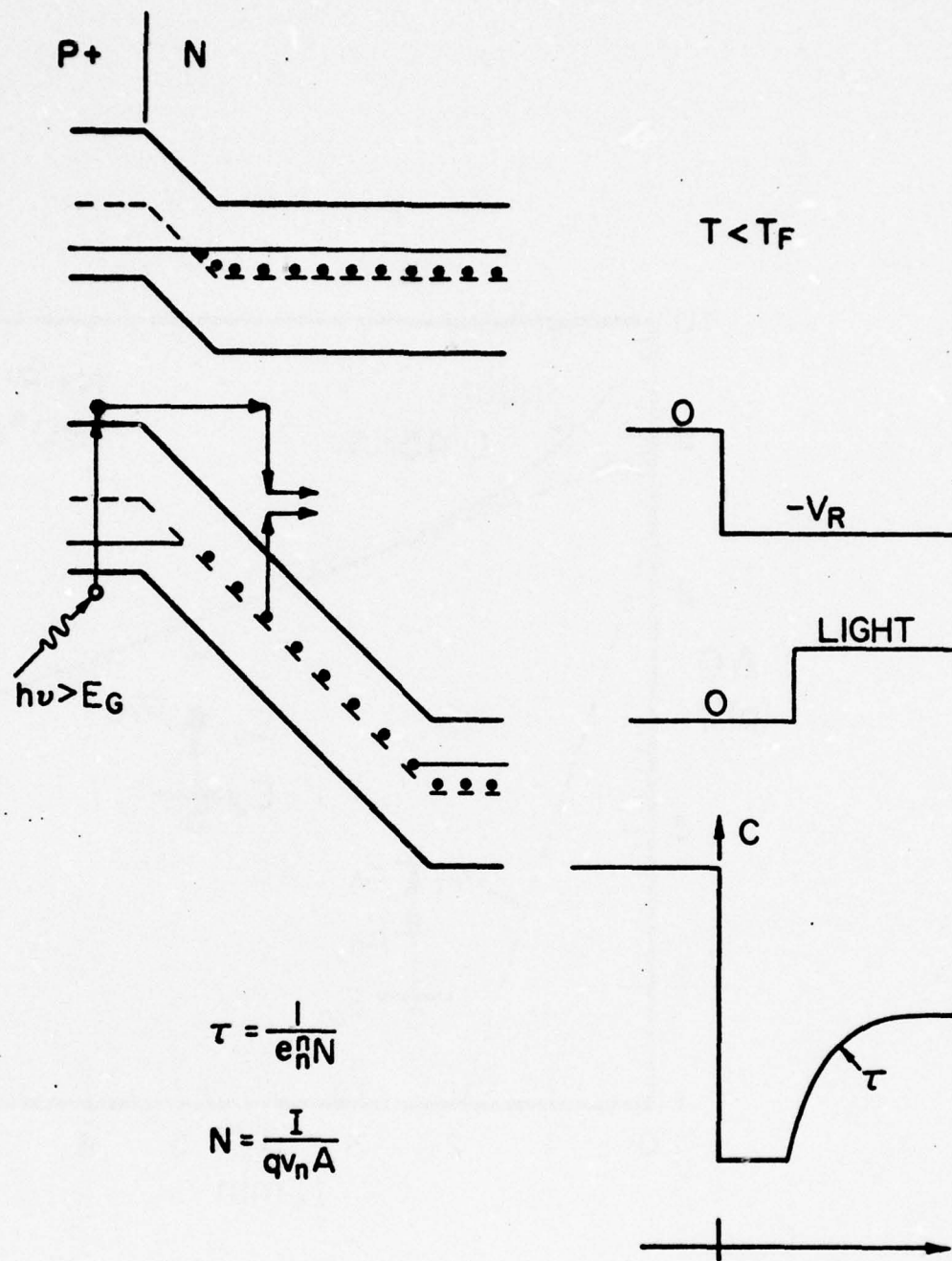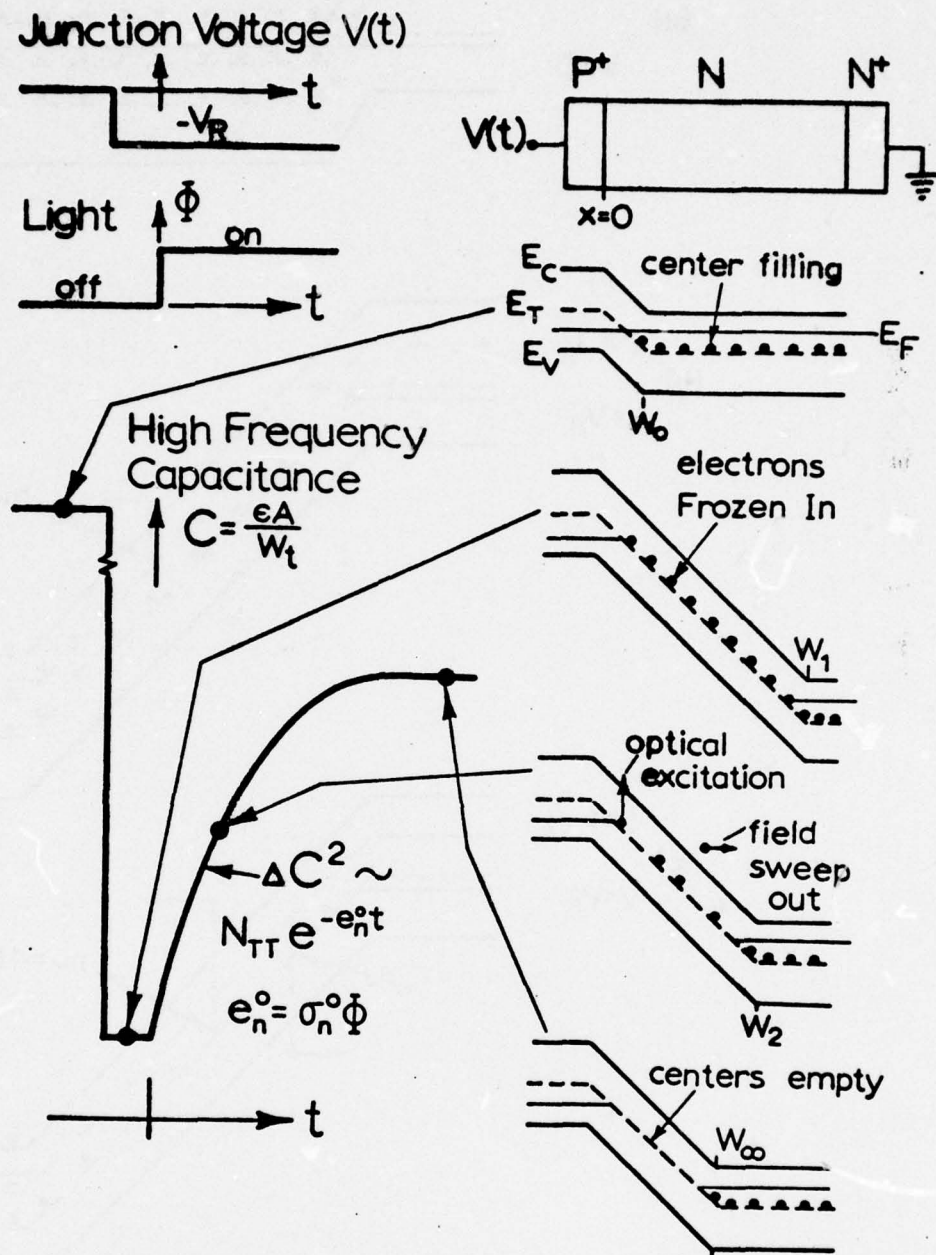
Figure 21. The energy band diagrams and the capacitance transient waveform illustrating a method of measuring the photo-ionization rate of an imperfection center or the optical emission rate of trapped electrons or holes.
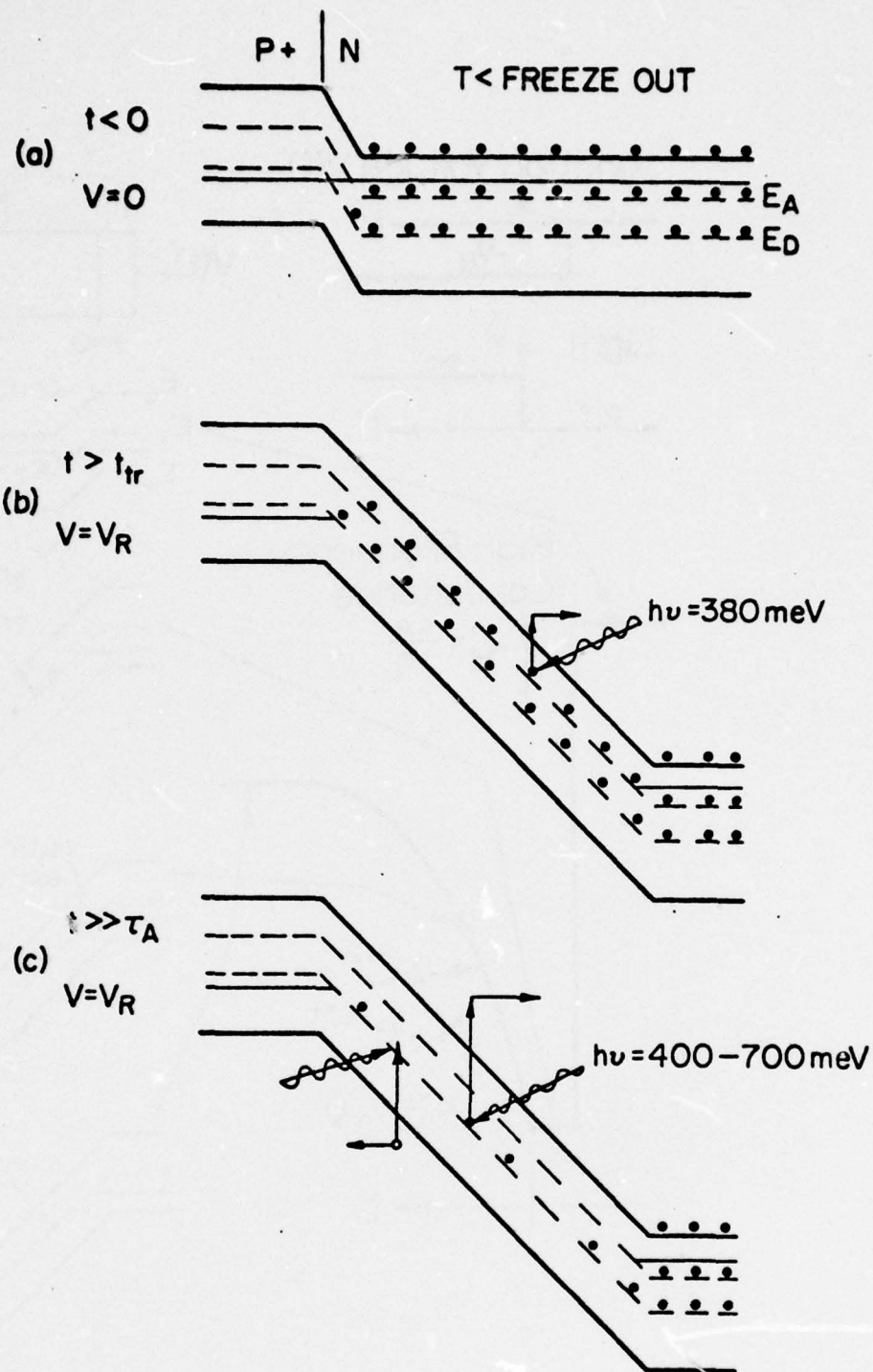
Figure 22. The energy band diagrams illustrating the sequence of exposure to monochromatic photons to get the optical emission rates of electrons trapped at a sulfur double donor center in silicon.

electrons. The higher energy photon (400-700 meV) is applied after the lower energy
one (380 meV). The two photocapacitance transients [5] are shown in Figure 23. The
approximately equal magnitude of the two capacitance transients is consistent with
the model that the two energy levels are from the same sulfur center in silicon.

As an illustration of the sensitivity of the photocapacitance method and
its use for fundamental studies, the photoionization cross section below the
extrinsic edge [13] is shown for the deeper one-electron sulfur level in Figure
24. The continum is at 613 meV labeled as (5). There are several humps in the
spectra below the threhold as indicated in the inset. They are identified with
two-step photo-thermal transitions from the ground state, $1s(A_1)$, to the excited
states. The first step is the optical transition and is indicated in the right
column in Figure 25, which also gives the theoretical one-electron energy levels
of sulfur in silicon on the left calculated from a pseudopotential theory [18],
and the published optical absorption spectra in the middle column. [13] For
example, the hump labeled (1) at 425 meV is attributed to a two-step process in
which the bound electron at the ground state, $1s(A_1)$, first makes an optical
transition to the excited state $1s(T_2)$ and is then thermally released into the
conduction band from the $1s(T_2)$. Humps (2) and (4) correspond to optical transi-
tions of $1s(A_1)$ to $2p_0$ and $1s(A_1)$ to $2p\pm$. The ledge at (3) can be attributed to
the optical transition $1s(A_1)$ to $2s(T_2)$.

3.5 Depletion Layer Thermally Stimulated Capacitance (TSCAP) [18]

and Current (TSC) [10]

When there are many imperfection levels in the band gap, one would like to
scan the gap quickly to sort them out before detailed measurements are made. [21,30]
Thermally stimulated capacitance (TSCAP) [19] or thermally stimulated current
(TSC) [10] data can provide this kind of information. Figure 26 shows the capaci-
tance versus temperature curves of the TSCAP experiment on a one-MeV electron

-37-
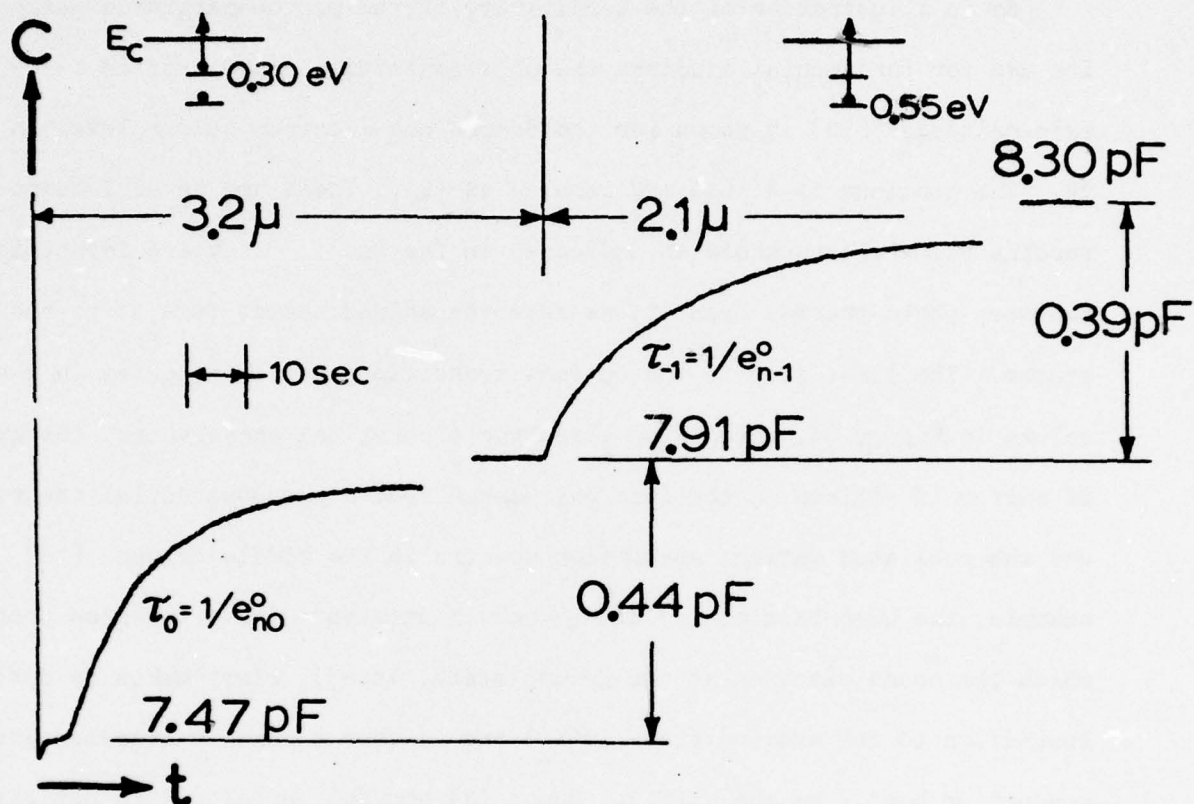
Figure 23. The observed photocapacitance transient from optical emission of the electrons trapped at the sulfur double donor center in silicon. Note that the total capacitance changes are essentially equal for the two transients supporting the idea that the two donor energy levels are from the same sulfur donor center. [5]
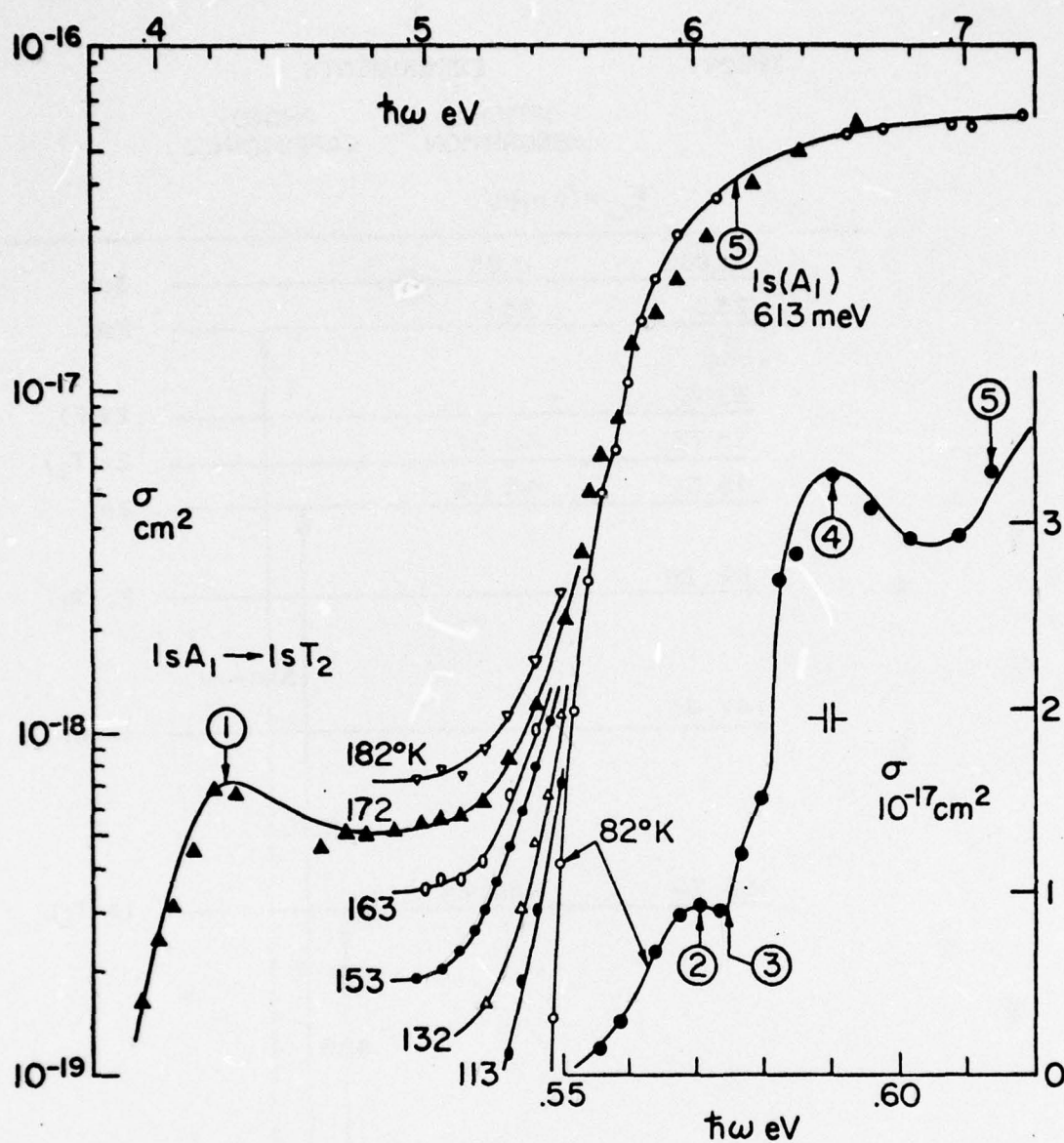
Figure 24. Highly sensitive measurement of the photoionization
cross section from the optical emission rate data of
the capacitance transient from electrons trapped at
the deep sulfur donor center in silicon at 613 meV
below the silicon conduction band edge. [13]
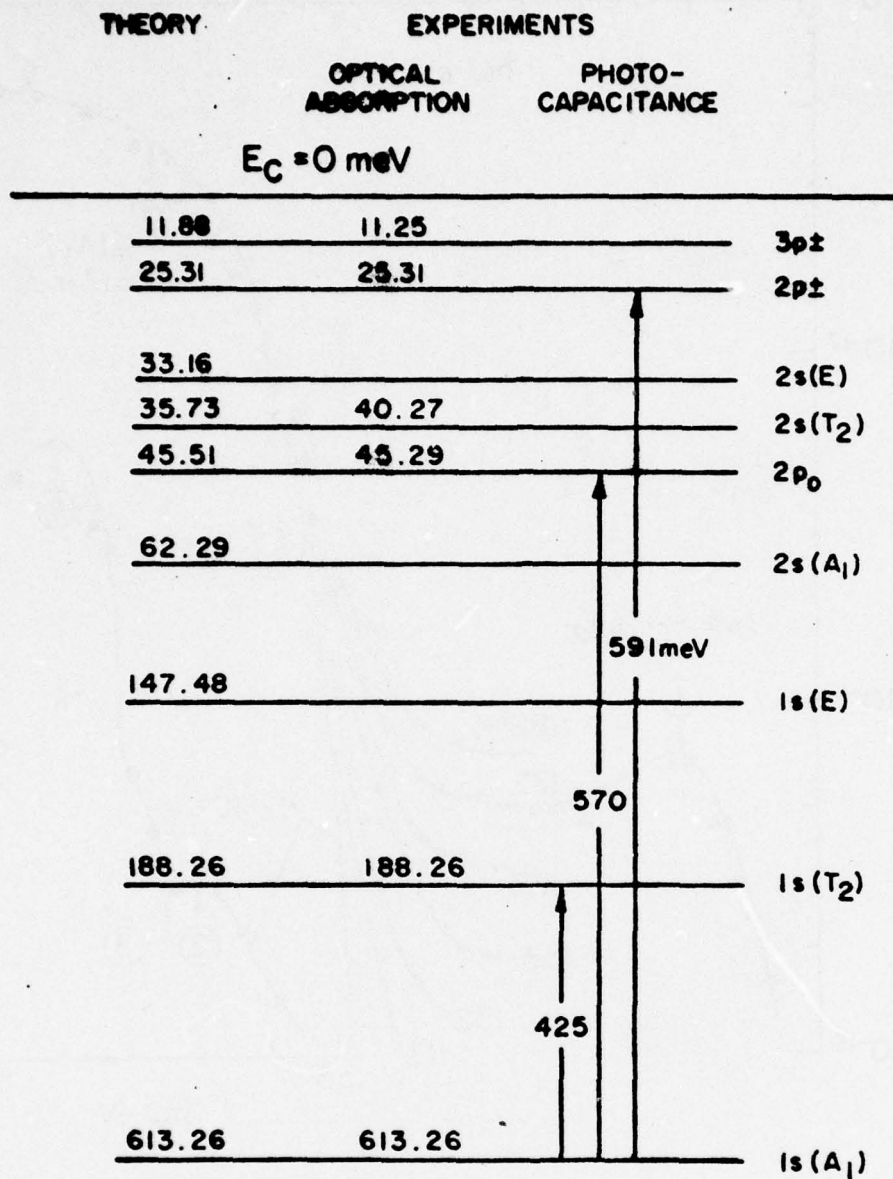
Figure 25. The calculated and observed energy levels of the one-electron sulfur donor center in silicon. [18]
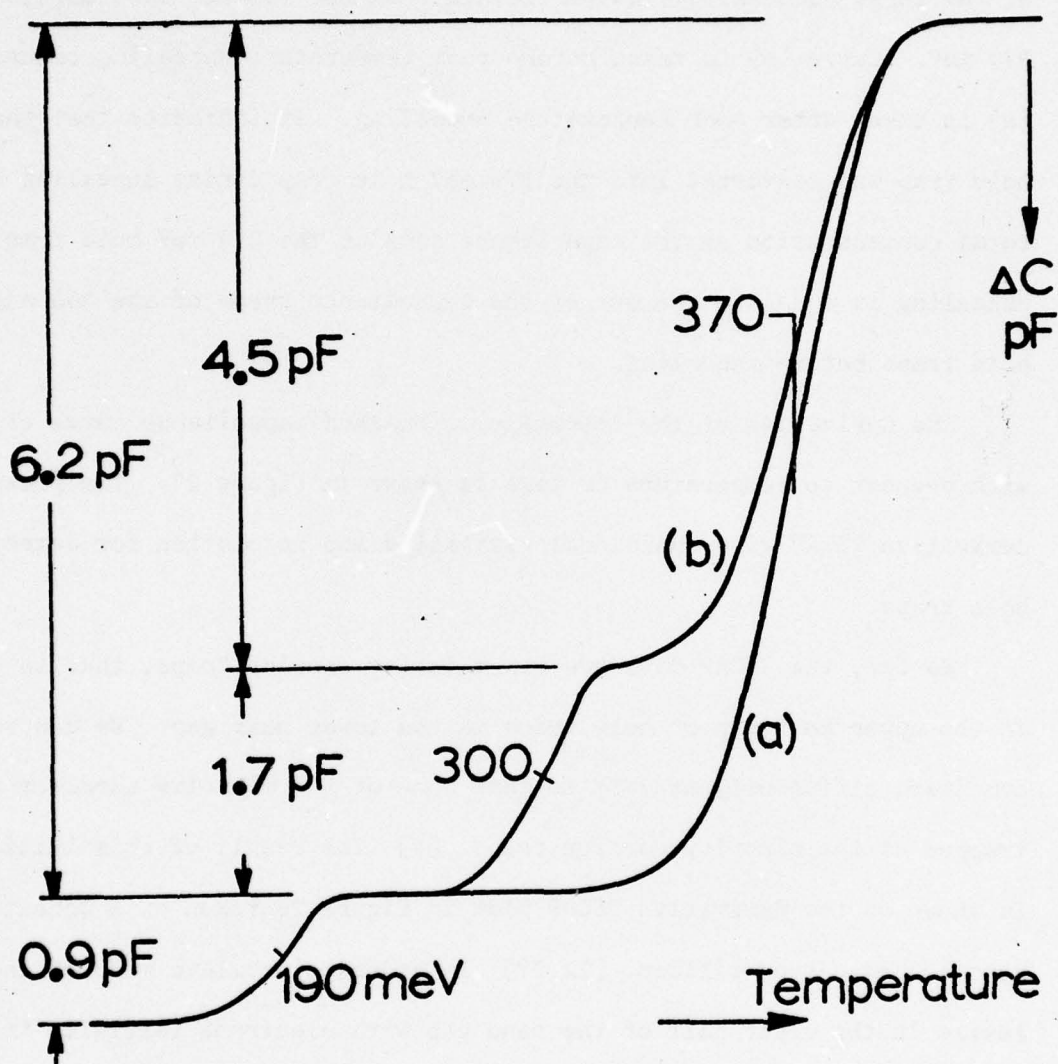
Figure 26. Example of scanning the band gap for the majority carrier traps by thermally stimulated capacitance measurements for defect centers produced by one MeV electron irradiation. [19]

irradiated silicon N+P junction. [30] The junction is first cooled to 77°K and then zero biased to fill the majority carrier trap with holes. The junction is then reverse biased and its temperature is increased linearly with time. The three capacitance steps in curve (b) correspond to emission of the trapped holes at the three successively deeper levels from the valence band edge, 190, 300 and 370 meV. Curve (b) is taken before room temperature annealing occurred. Curve (a) is taken after room temperature annealing. It indicates that the 300 meV hole trap was converted into the 370 meV hole trap during annealing since the total concentration or the capacitance step of the 370 meV hole trap after annealing is equal to the sum of the capacitance steps of the 300 and 370 meV hole traps before annealing.

The derivative of the thermally stimulated capacitance curve of Figure 26 with respect to temperature or time is shown in Figure 27. The peaks of the derivative TSCAP give additional visibility and resolution for detecting the hole traps.

So far, the TSCAP data are for majority carrier traps, that is electron traps in the upper half gap or hole traps in the lower half gap. We can set the initial condition differently at 77°K so that some of the minority carriers are also trapped at the minority carrier traps. [7] The result of this initial condition is shown on the derivative TSCAP plot in Figure 28 taken on a Cobalt doped junction on p-type silicon. [22,27] In order to populate some of the Co acceptor levels in the upper half of the band gap with electrons initially in the p-type region, the reverse biased junction is exposed to a monochromatic light of about one micron wavelength (1.24 eV) at 77°K. [27] This phtotexcitation causes some electrons to be trapped at the Co acceptor level. The derivative TSCAP is then taken. Note that a peak is obtained at 140°K for the majority carriers, holes, trapped at the Co donor level which is located in the lower half of the band gap

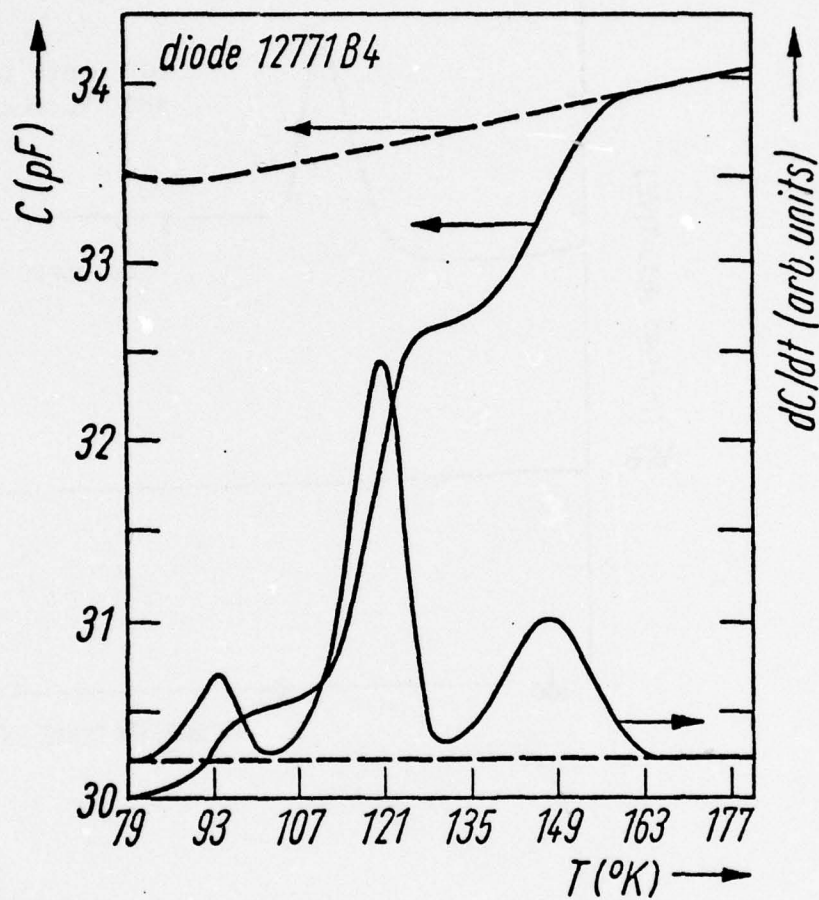Figure 27. The time or temperature derivative of the thermally stimulated capacitance as a function of temperature of the device shown in Figure 26.
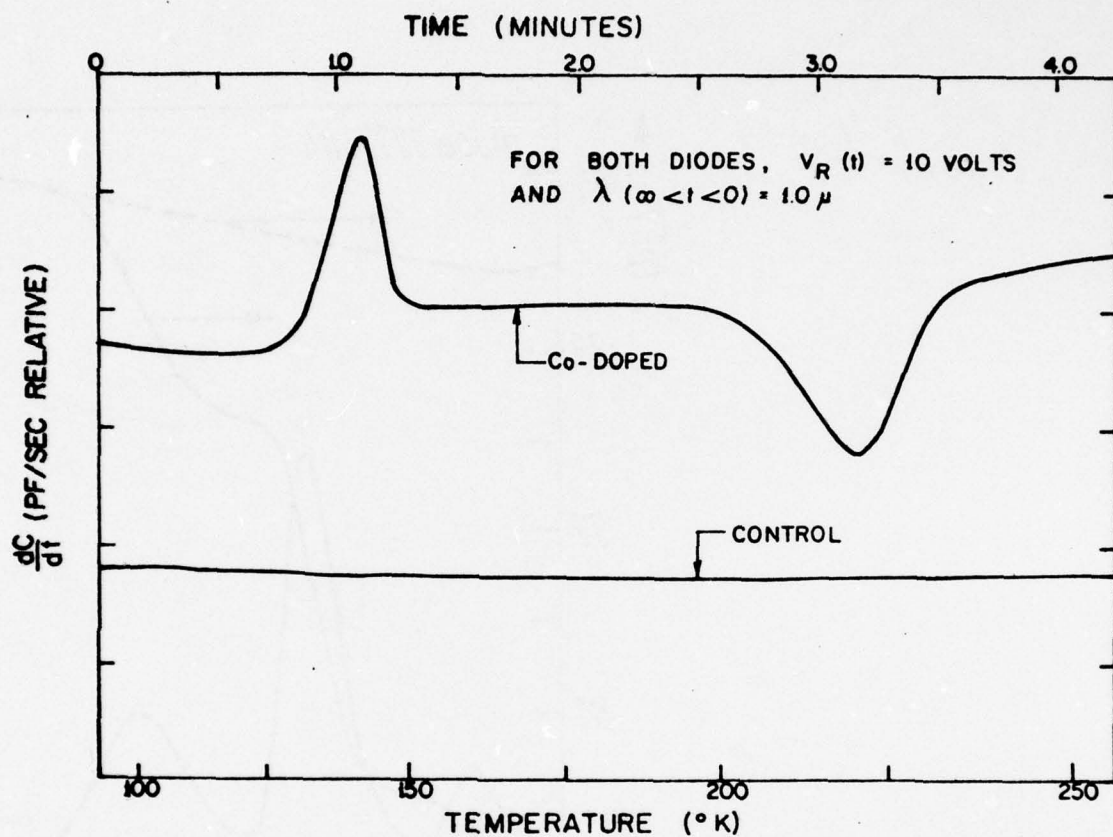
Figure 28. Experimental derivative TSCAP data illustrating the detection of both a majority carrier and a minority carrier trap in Cobalt-doped junction on p-type silicon. [27]

-44-

at 377 meV above the valence band edge. However, a minimum is observed at 240°K for the electrons (minority carriers in p-Si) trapped at the acceptor level which is located in the upper half of the band gap at 569 meV below the conduction band edge.

An example of using the thermally stimulated junction current (TSC) to scan the band gap for defect levels produced by ion implantation is shown in Figure 29 taken on a junction on p-type silicon. This method gives current peaks for both the majority and minority carrier traps. Thus, it cannot distinguish the majority carrier (hole) traps in the lower half of the band gap from the minority carrier (electron) traps in the upper half of the band gap. Only the capacitance tran- sients given on the upper part of the figure can tell whether the level is a majority or minority carrier trap. Those with negative signs are from minority carrier traps in the upper half gap and those with positive signs are from majority carrier traps in the lower half gap. The current is low and its measure- ment require very careful shielding. In contrast, the capacitance measurements require little or no special shielding since the capacitance bridge employs a phase sensitive detector.

3.6 Edge Layer Thermally Stimulated Capacitance [29]

The range of the band gap that can be scanned by the depletion layer TSCAP or TSC method just discussed is determined by the starting temperature. For liquid nitrogen temperature, this is about 200 meV from a band edge so that shallower level traps are missed unless lower temperature is used. This is not very convenient since it requires liquid helium facility.

However, there is another capacitance change which can reach closer to the band edge at 77°K than the depletion layer TSCAP. This capacitance change comes from emptying or filling of the traps in the edge region of the p-n junction
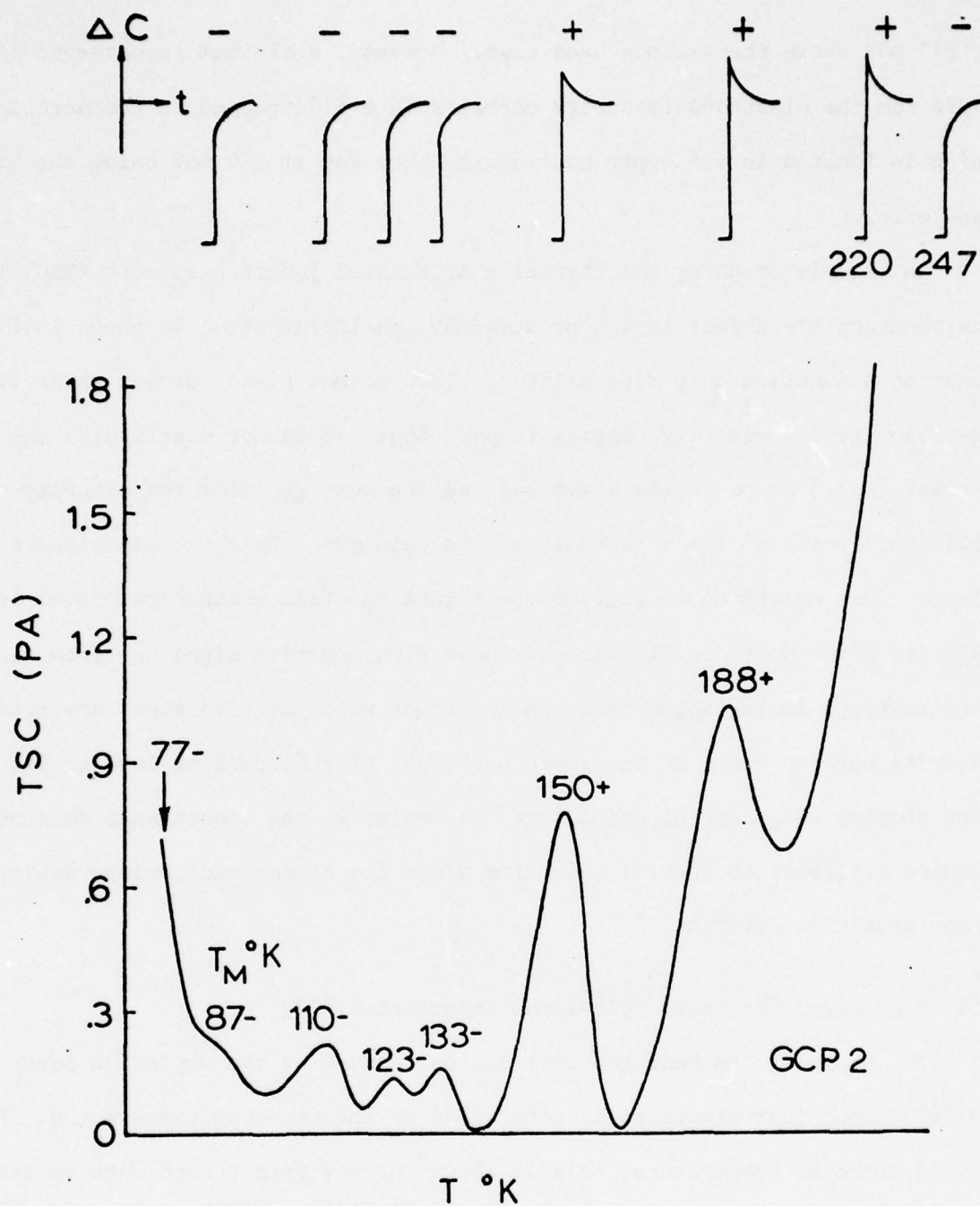
Figure 29. An example of the use of thermally stimulated junction current (TSC) versus temperature to scan the band gap for defect levels produced by implantation of 150 KeV boron ions. [Unpublished]

when the bulk Fermi level crosses these trap levels as the temperature is increased. [29]

This is known as the *edge layer* thermally stimulated capacitance effect. It is illustrated in Figure 30. Process (1) is the usual *depletion layer* TSCAP while process (2) gives the *edge layer* TSCAP. The edge region TSCAP can reach levels as close as 60 meV from a band edge at 77°K compared with the 200 meV from the depletion region TSCAP.

Data of the edge layer TSCAP [29] is illustrated in Figure 31. Curve b is the depletion layer TSCAP with the condition that the traps are initially filled with electrons at 30°K. The peak at 70°K is due to the A-center or oxygen-vacancy pair which is 174 meV below the conduction band edge. Curve a is obtained without zero biasing the junction so that all the traps in the depletion layer are initially empty and would not give capacitance changes with temperature. The edge region, however, will give capacitance changes with temperature as illustrated by the 149°K peak in the lower right figure since the traps in the edge region are filled initially even without zero bias. This peak at 149°K gives a defect level at 180 meV below the conduction band edge which is in good agreement with the energy level, 174 meV, of the A-center from the depletion layer TSCAP at 70°K obtained above.

3.7 Capacitance and Current Transients in MOS Capacitors [20,24]

Let us next briefly discuss the capacitance and current transients that can be observed in reverse biased and depleted surface space charge region of MOS capacitors. [20] The main difference in the capacitance transients between a MOS capacitor and a p-n junction or Schottky barrier is that the insulator-semiconductor interface of the MOS capacitor can accumulate minority carriers which are generated in the space charge region while there is no potential well in p-n junctions or Schottky barriers to retain the minority carriers.
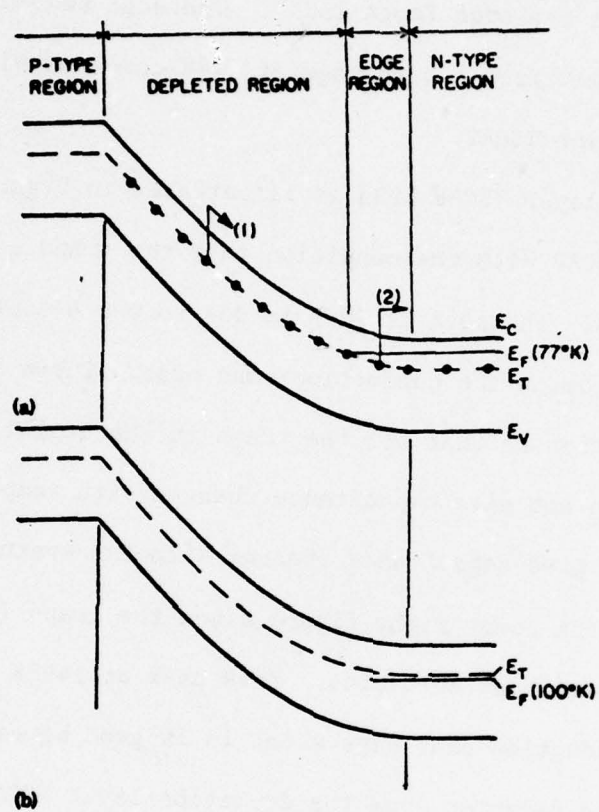
-47-

Figure 30. The energy band diagram illustrating the use of the edge region TSCAP effect to reach shallower traps at or above liquid nitrogen temperature. [29]
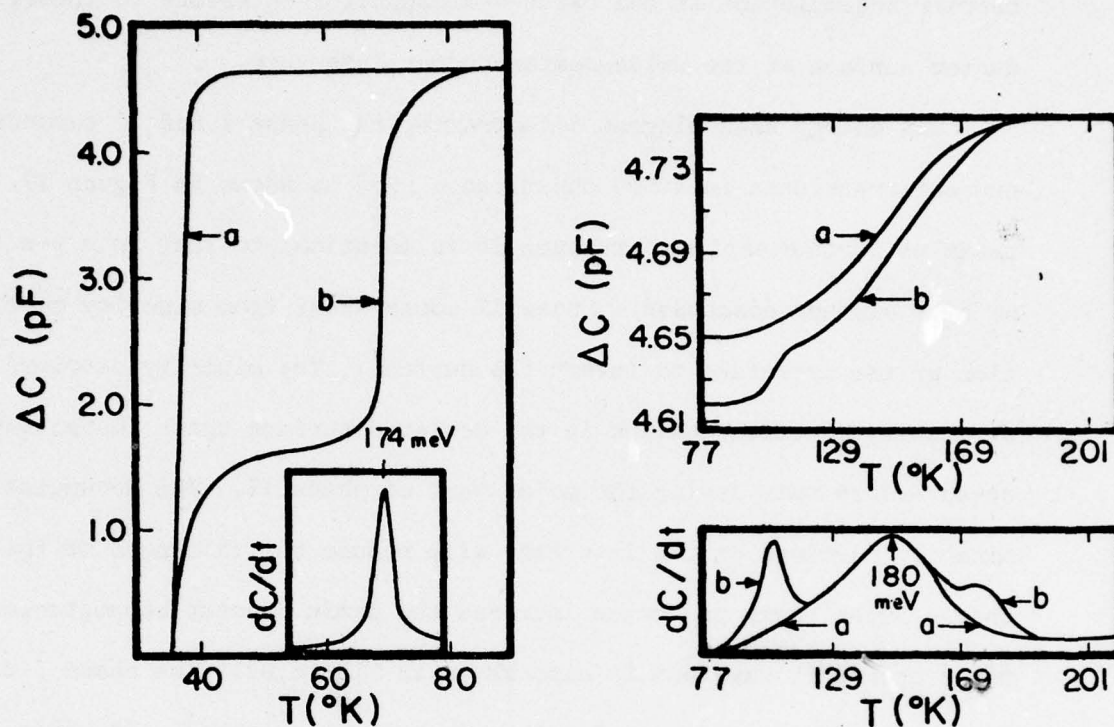
Figure 31.   TSCAP curves of electron irradiated silicon p-n junction
illustrating a shallow donor level whose depletion layer
TSCAP peaked at about 70°K while its edge layer TSCAP
peaked at about 149°K. [29]

-49-

The capacitance and current transients in MOS capacitors can be divided into two phases with widely different time constants. Phase I is identical to that observed in a p-n junction. The much slower phase II arises from minority carrier accumulation at the oxide-semiconductor interface to invert the semiconductor surface at the oxide-semiconductor interface.

The energy band diagram illustrating the phase I and II capacitance and current transients in a MOS capacitance [20] is shown in Figure 32. Phase I needs no further explanation since it is identical to that in a p-n junction which we have already discussed. Phase II comes about from minority carrier accumulation at the interface to invert the surface. The minority carriers are generated at the imperfection centers in the depleted surface space charge layer at a steady-state rate during the major part of phase II. The accumulation of the minority carriers at the interface will reduce the thickness of the surface space charge layer width and hence increase the semiconductor capacitance. The capacitance transient waveform is also shown in Figure 32. The phase I capacitance change is usually much smaller than we have illustrated. Its size is proportional to the trap concentration in the surface space charge layer. Thus, we can use the phase I transient to determine all the properties obtainable for a p-n junction such as the emission rate of the majority carriers and the trap concentration. Phase II gives additional information. The phase II time constant is inversely proportional to the thermal emission rate of the *minority* carriers while phase I is equal to reciprocal of the *majority* carrier emission rate. These are summarized below.

$$\tau_I = \frac{1}{e_n + e_p} \simeq \frac{1}{e_p} \qquad \text{for p-Si, } e_p >> e_n \tag{9}$$

$$\frac{\Delta C_I}{C_I} = \frac{N_{TT}}{2N_{AA}} \tag{10}$$
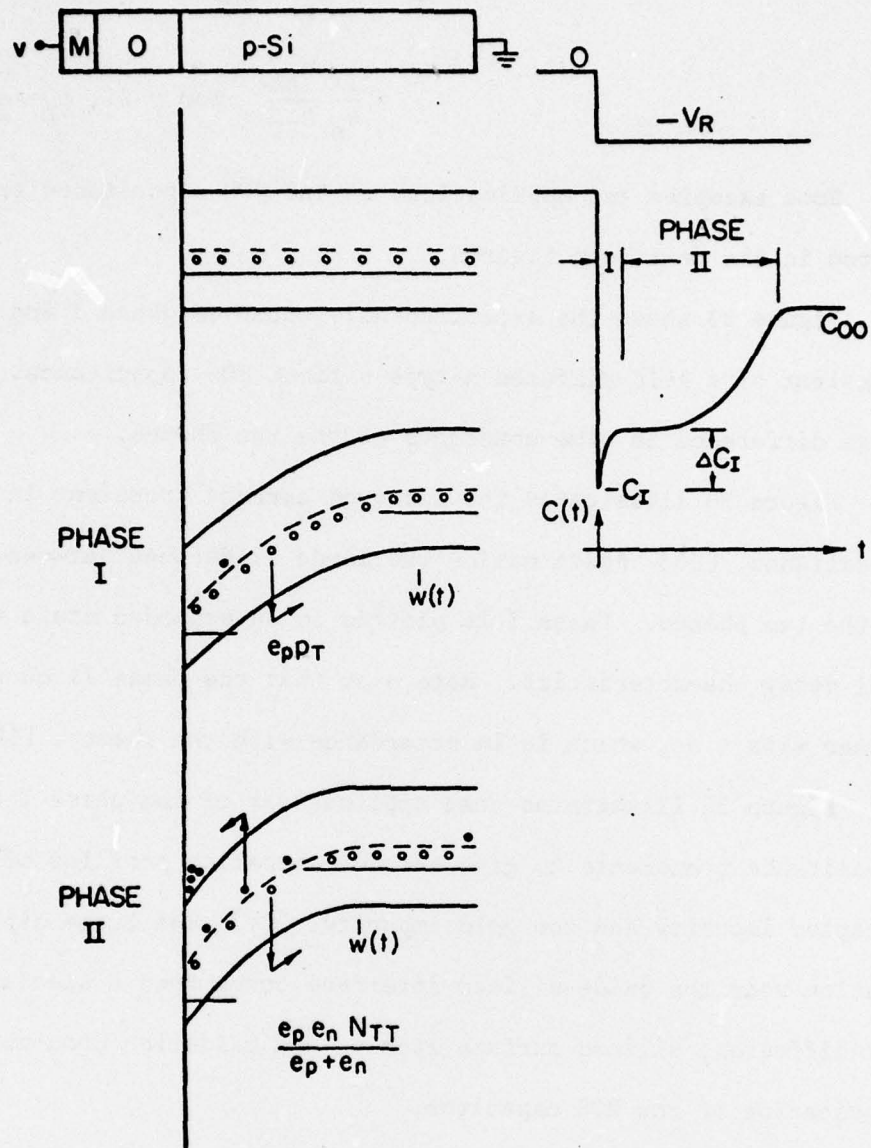
-50-

MOS CAPACITANCE TRANSIENT

Figure 32. Energy band diagrams and capacitance transient waveform illustrating phase I and II capacitance and current transients after the MOS capacitor is switched from flat-band to a reverse bias. [20,24]

$$\tau_{II} = \frac{e_n + e_p}{e_n e_p} \frac{N_{AA}}{N_{TT}} \tag{11}$$

$$\simeq \frac{1}{e_n} \frac{N_{AA}}{N_{TT}} \quad \text{for p-Si, } e_p >> e_n \tag{11A}$$

Some examples and applications of the MOS capacitance transients are illustrated in the next four figures.

Figure 33 shows the experimentally observed phase I and II capacitance transient of a gold-diffused n-type silicon MOS capacitance. [20] Notice the large difference in time constants of the two phases.

Figure 34 illustrates the observed current transient in a gold-diffused MOS capacitance. [20] Again notice the large difference between the time constants of the two phases. Phase I is plotted in an expanded scale to show its exponential decay characteristics. Note also that the phase II current decay is nearly linear with time, which is in accordance with the theory. [20]

Figure 35 illustrates some applications of the phase I and phase II MOS capacitance transients to give the concentration proflies of both the boron acceptor impurity and the gold impurity. [24] The large dip of the gold concentration near the oxide-silicon interface comes from a special sequence of gold out-diffusion, silicon surface etching and oxidation procedure used in the fabrication of the MOS capacitor.

Figure 36 shows another useful application of the phase II capacitance transient. [24] The vertical axis is essentially the reciprocal of the phase II time constant. The values of the variable along the vertical axis can be obtained directly from the second derivative of the experimental phase II capacitance-time curve. The data show that there is a small region of high minority carrier generation rate at about 2.5 microns from the interface. The rapid increase of the phase II rate constant with increasing depth is not due to a rise of the

PHASE I

$\tau_I \simeq \dfrac{1}{e_n^t}$

$N_{DD} = 5 \times 10^{14} \, P/cm^3$

$N_{Au} = 2 \times 10^{14} \, Au/cm^3$

PHASE II

$\tau_{II} \simeq \dfrac{N_{DD}}{e_p^t N_{Au}}$

5

CAPACITANCE (pF)

10

T = 231.85 K

15

0   1   2   3

t (min)
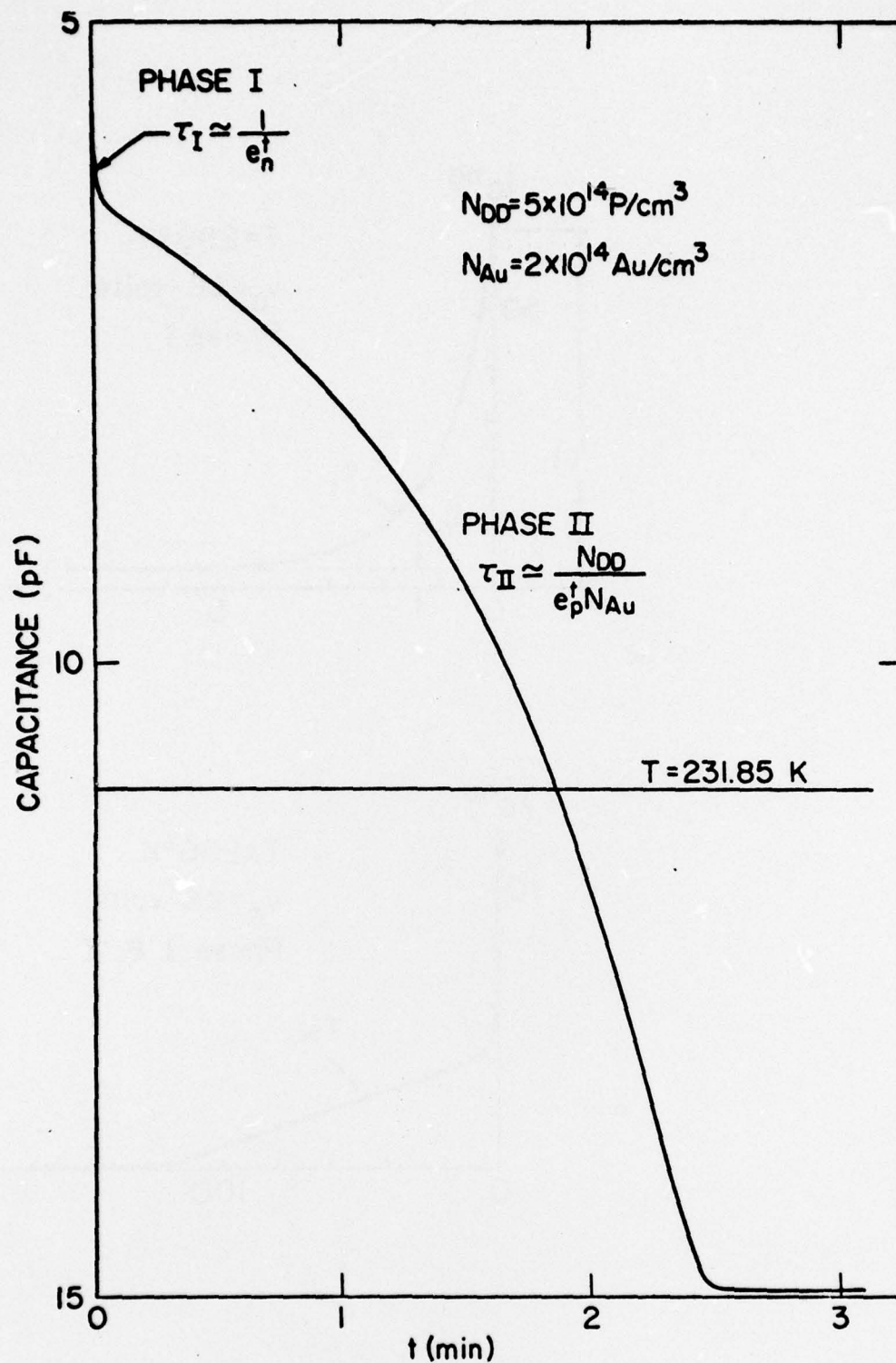
Figure 33. Experimental curve illustrating the observed capacitance
transient waveform during phase I and phase II after
the MOS capacitor is switched to reverse bias. [20]

-53-
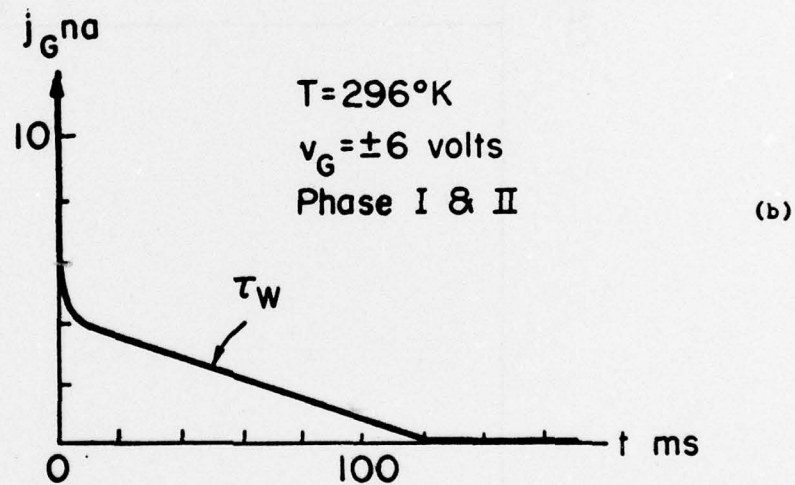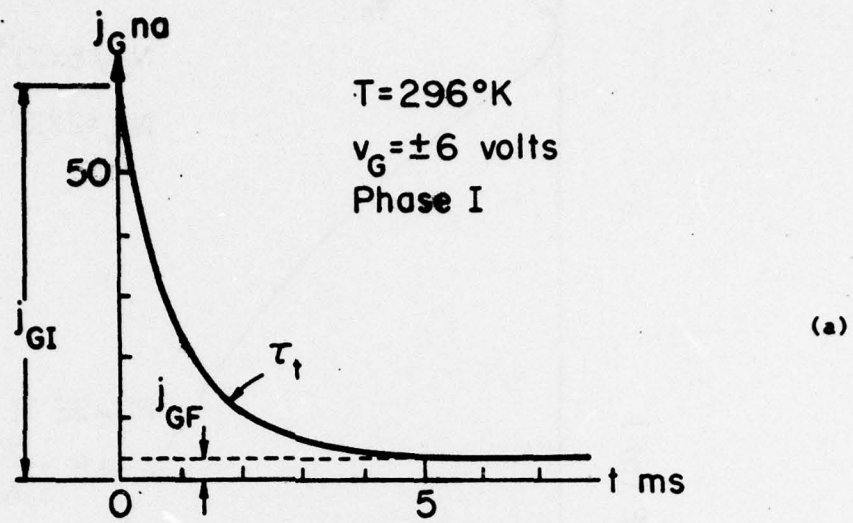
Figure 34. The current waveform after the MOS capacitor is switched to a reverse bias, illustrating both the phase I and II transients. [20]
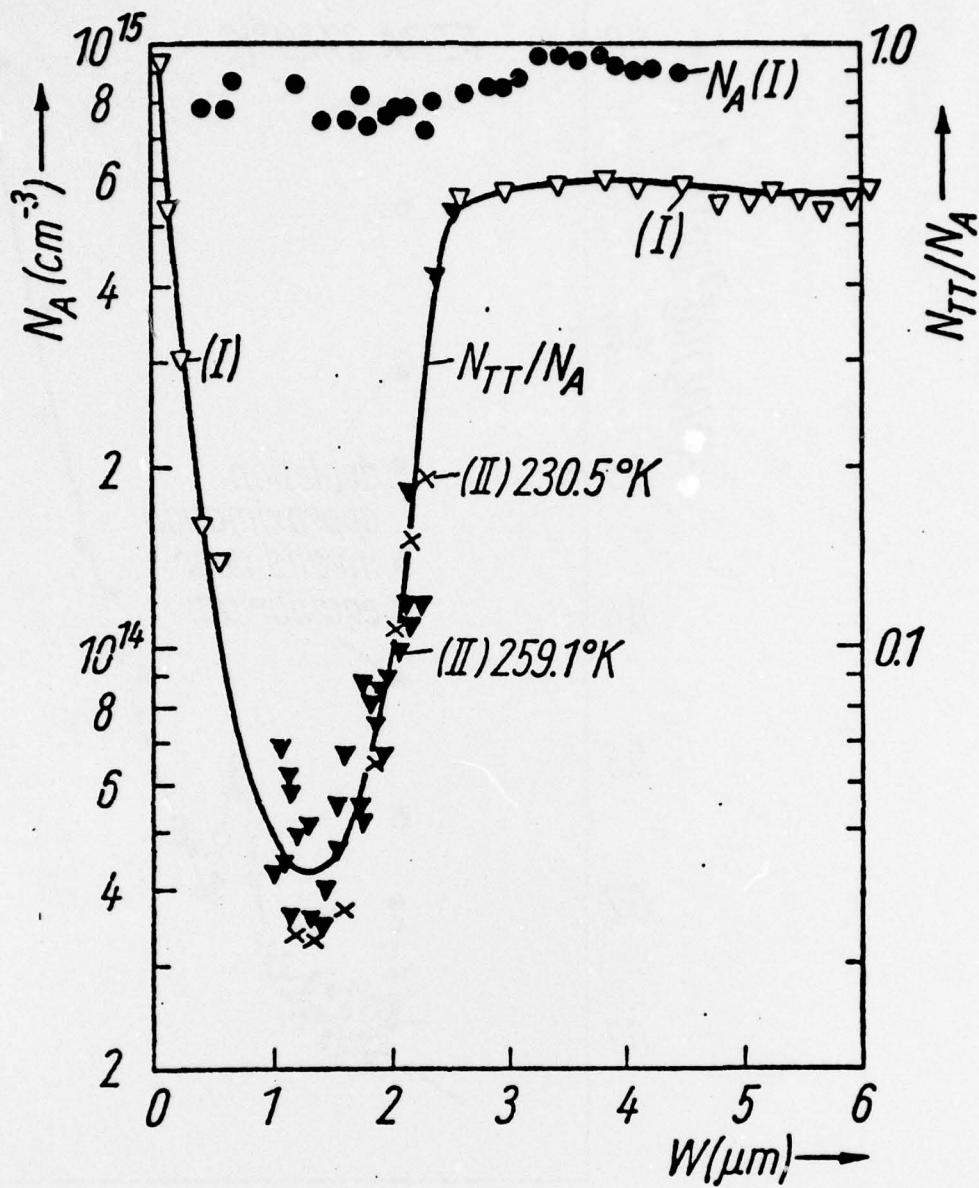
Figure 35. An example of using the phases I and II MOS capacitance transients to obtain the majority doping acceptor or boron profile and the profile of the gold concentration in the surface space charge layer. [24]
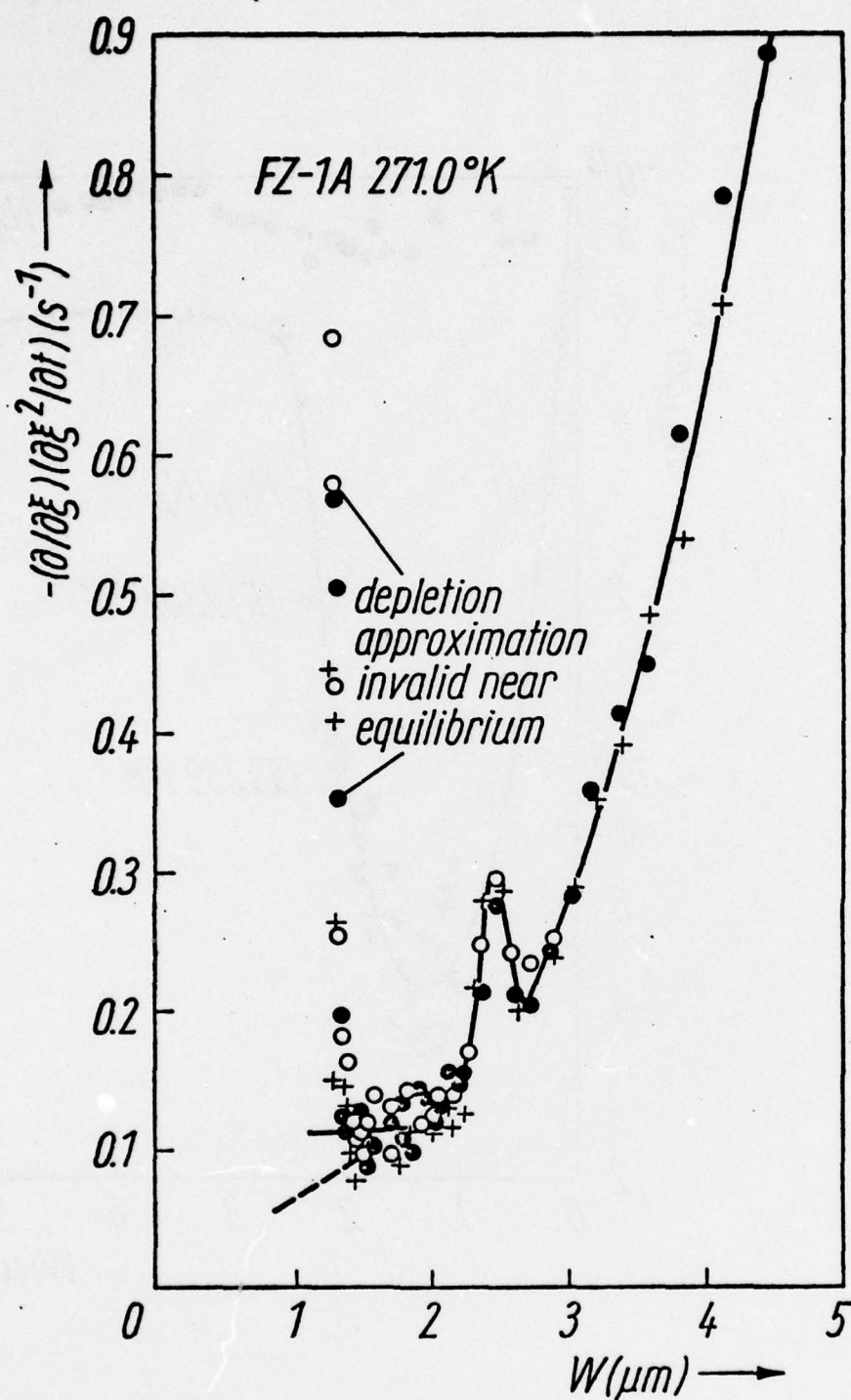
Figure 36. The second derivative of the phase II MOS capacitance transient versus position from the oxide-silicon interface showing a defect of high generation rate at 2.5 microns from the interface. [24]

trapping center density nor a decrease of the boron concentration in the interior as indicated by Equations (9) to (11). Instead, it shows the large increase of the minority carrier generation rate with increasing electric field as the junction depth is increased. This is similar to the softness of the reverse characteristics of p-n junction.

An important direct application of the generation rates obtained from the MOS phase II or inversion time constant is its use in the calculation of leakage current of an adjacent junction in a IC chip and in the prediction of the maximum refresh time in CCD.

IV. SUMMARY AND ACKNOWLEDGEMENT

Some of the eight new techniques, using the space charge layer of a p-n junction, Schottky barrier and a MOS capacitor to determine the properties of imperfection centers, are discussed. These are the depletion layer dark and photo current and capacitance transients, the edge layer dark and photo capacitance transients, the thermally stimulated current and capacitance. A variety of initial charge states of the traps can be set by switching the junction bias, using thermal or photo excitation of the trapped charges, and by injection of the photogenerated carriers on the surface or by injection from a forward biased emitter junction.

These new measurement techniques will provide extensive and accurate data on the kinetic parameters of the recombination, generation and trapping processes to improve our understanding of the bound states in semiconductors. They can also be used to monitor silicon integrated circuit processes. An extensive investigation of the process (thermally) generated recombination centers in silicon at high temperatures has recently been made using these techniques. [39]

-57-

CHRONOLOGICAL BIBLIOGRAPHY

1. C. T. Sah and A. F. Tasch, "Precise determination of the multiphonon and photon carrier generation properties using the impurity photovoltaic effect in semiconductors," Phys. Rev. Letts., v19, No. 2, 69-71, 10 July 1967.

2. C. T. Sah, A. F. Tasch, and D. K. Schroder, "Recombination properties of the gold acceptor level in silicon using the impurity photovoltaic effect," Phys. Rev. Letts., v19, No. 2, 71-72, 10 July 1967.

3. C. T. Sah, L. Forbes, L. L. Rosier, A. F. Tasch, Jr., and A. B. Tole, "Thermal emission rates of carriers at gold centers in silicon," Appl. Phys. Letts., v15, No. 5, 145-148, 1 September 1969.

4. C. T. Sah, L. L. Rosier, and L. Forbes, "Low-temperature high-frequency capacitance measurements of deep-and shallow-level impurity center concentrations," Appl. Phys. Letts., v15, No. 5, 161-164, 15 September 1969.

5. C. T. Sah, L. L. Rosier and L. Forbes, "Direct observation of the multiplicity of impurity charge states in semiconductors from low-temperature high-frequency photocapacitance," Appl. Phys. Letts., v15, No. 10, 316-318, 15 November 1969.

6. A. F. Tasch, Jr. and C. T. Sah, "Recombination-generation and optical properties of gold acceptor in silicon," The Physical Review B, v1, No. 2, 800-809, 15 January 1970.

7. C. T. Sah, L. Forbes, L. L. Rosier and A. F. Tasch, Jr., "Thermal and optical emission and capture rates and cross sections of electrons and holes at imperfection centers in semiconductors from photo and dark junction current and capacitance experiments," Solid-State Electronics, v13, 759-788, June 1970.

8. T. H. Ning and C. T. Sah, "Multi-valley and effective-mass approximation of shallow donor levels in silicon," Solid-State Communications, v8, 1893-1897, November 1970.

9. L. L. Rosier and C. T. Sah, "Thermal emission and capture of electrons at sulfur centers in silicon," Solid-State Electronics, v14, 41-54, January 1971.

10. L. Forbes and C. T. Sah, "On the determination of deep level center energy and concentration by thermally stimulated conductivity measurements using reverse-biased p-n junctions, Solid-State Electronics, v14, 182-183, February 1971.

11. C. T. Sah, L. Forbes, L. L. Rosier and A. F. Tasch, Jr., "Thermal and optical emission rates and cross sections from the impurity photocurrent and photo-capacitance methods," Proc. Third Int. Conf. Photoconductivity, 253-258, Editor: E. M. Pell, Pergamon Press, New York (1971).

12. T. H. Ning and C. T. Sah, "Group-VI donor impurities in silicon," Physics Letters, v35A, No. 4, 238-239, 14 June 1971.

13. C. T. Sah, T. H. Ning, L. L. Rosier, and L. Forbes, "Photothermal ionization via excited states of sulfur donor in silicon," Solid State Communications, v9, 917-920, 15 June 1971.

14. L. D. Yau and C. T. Sah, "Thermal ionization rates and energies of electrons and holes at silver centers in silicon," phys. stat. sol. (a), v6, 561-573, 16 August 1971.

15. L. L. Rosier and C. T. Sah, "Photoionization of electrons at sulfur centers in silicon," J. of Appl. Phys., v42, No. 10, 4000-4005, September 1971.

16. W. W. Chan and C. T. Sah, "Defect centers in boron-implanted silicon," J. of Appl. Phys., v42, No. 12, 4768-4773, November 1971.

17. T. H. Ning and C. T. Sah, "Multivalley effective-mass approximation for donor states in silicon. I. Shallow-level group-V impurities," Phys. Rev. B, No. 10, 3468-3481, 15 November 1971, see also reference 37.

18. T. H. Ning and C. T. Sah, "Multivalley effective-mass approximation for donor states in silicon. II. Deep-level group-VI double-donor impurities," Phys. Rev. B, v4, No. 10, 3482-3488, 15 November 1971, see also reference 38.

19. C. T. Sah, W. W. Chan, H. S. Fu, and J. W. Walker, "Thermally stimulated capacitance (TSCAP) in p-n junctions," Appl. Phys. Letts., v20, No. 5, 193-195, 1 March 1972.

20. C. T. Sah and H. S. Fu, "Current and capacitance transient responses of MOS capacitor. I. General theory and applications to initially depleted surface with surface states," phys. stat. sol. (a), v11, 297-310, 16 May 1972.

21. J. W. Walker and C. T. Sah, "Properties of 1 MeV electron-irradiated defect centers in p-type silicon," phys. stat. sol. (a), v11, 513-521, 16 June 1972.

22. L. D. Yau and C. T. Sah, "Measurement of trapped-minority-carrier thermal emission rates from Au, Ag, and Co traps in silicon," Appl. Phys. Lett., v21, No. 4, 157-158, 15 August 1973.

23. L. D. Yau, C. F. Smiley, and C. T. Sah, "Thermal emission rates and activation energies of electrons and holes at silver centers in silicon," phys. stat. sol. (a), v13, 457-464, 16 October 1972.

24. C. T. Sah and H. S. Fu, "Current and capacitance transient responses of MOS capacitor. II. Recombination centers in the surface space charge layer," phys. stat. sol. (a), v14, 59-70, 16 December 1972

25. J. M. Herman III and C. T. Sah, "Thermal ionization rates and energies of holes at the double acceptor zinc centers in silicon," phys. stat. sol. (a), v14, 405-415, 16 December 1972.

26. Sokrates Pantelides and C. T. Sah, "Theory of impurity states in semiconductors," Solid State Communications, v11, 1713-1718, 1 December 1972, see also references 37 and 38.

27. L. D. Yau, W. W. Chan, and C. T. Sah, "Thermal emission rates and activation energies of electrons and holes at cobalt centers in silicon," phys. stat. sol (a), v14, 655-662, 16 December 1972.

28. J. M. Herman III and C. T. Sah, "Photoionization cross sections of holes at zinc centers in silicon, J. Appl. Phys., v44, No. 3, 1259-1262, 1 March 1973.

29. C. T. Sah and J. W. Walker, "Thermally stimulated capacitance for shallow majority-carrier traps in the edge region of semiconductor junctions," Appl. Phys. Letts., v22, No. 8, 384-385, 15 April 1973, see also reference 36.

30. J. W. Walker and C. T. Sah, "Properties of 1 MeV electron-irradiated defect centers in silicon," Physical Review B, v7, 4587-4605, 15 May 1973.

31. J. M. Herman III and C. T. Sah, "Thermal capture of electrons and holes at zinc centers in silicon," Solid-State Electronics, v18, 1133-1139, 1 October 1973.

32. J. W. Walker and C. T. Sah, "Spherical square well defect potential model for one MeV electron irradiated defects in silicon," Physical Review B, v8, 5597-5603, 15 December 1973.

33. J. W. Walker and C. T. Sah, "Characteristics of 1 MeV electron-irradiated surface-controlled silicon junction diodes," Radiation Effects, v20, 187-195, 1973.

34. L. D. Yau and C. T. Sah, "Quenched-in centers in silicon p+n junctions," Solid-State Electronics, v17, 193-201, February 1974.

35. C. T. Sah, "Equivalent circuit models in semiconductor transport for thermal, optical, Auger-impact and tunneling recombination-generation-trapping processes," phys. stat. sol. (a), v7, 541-559, 16 October 1971.

36. C. T. Sah, C. T. Wang and S. H. Lee, "Junction edge region thermally stimulated capacitance (TSCAP) of n-Si doped with phosphorus and bismuth," Appl. Phys. Letts., v25, 523, 1 November 1974.

37. S. T. Pantelides and C. T. Sah, "Theory of localized states in semiconductors. I. New results using an old method," Phys. Rev. B, v10, No. 2, 621-637, 15 July 1974.

38. S. T. Pantelides and C. T. Sah, "Theory of localized states in semiconductors. II. The pseudo impurity theory application to shallow and deep donors in silicon," Phys. Rev. B, v10, No. 2, 638-658, 15 July 1974.

39. C. T. Sah and C. T. Wang, "Experiments on the origin of process-induced recombination centers in silicon, J. of Appl. Phys., v46, 1767-1776, 1 April 1975.

40. K. Miyata and C. T. Sah, "Thermal emission rates and activation energies of electrons at tantalum centers in silicon," Solid-State Electronics, v19, 611-613, 01 July 1976

41. T. H. Ning and C. T. Sah, "Photoionization cross sections of a two-electron center in silicon," Phys. Rev. v14, 2528-2533, 15 September 1976

42. C. T. Sah and A. Neugroschel, "Concentration profiles of recombination centers in semiconductor junction evaluated from capacitance transients," IEEE Trans. Electron Devices, vED-23, 1069-1074, 01 September 1976

43. R. Marchand and C. T. Sah, "Studies of thermally induced deep levels in Al-doped silicon, Journal of Applied Physics, v47, 1-10, 01 January 1977.

MISSION
of
Rome Air Development Center

RADC plans and conducts research, exploratory and advanced development programs in command, control, and communications (C^3) activities, and in the C^3 areas of information sciences and intelligence. The principal technical mission areas are communications, electromagnetic guidance and control, surveillance of ground and aerospace objects, intelligence data collection and handling, information system technology, ionospheric propagation, solid state sciences, microwave physics and electronic reliability, maintainability and compatibility.